HHS Public Access

Author manuscript

Cell Rep. Author manuscript; available in PMC 2025 May 27.

Published in final edited form as:

Cell Rep. 2024 August 27; 43(8): 114624. doi:10.1016/j.celrep.2024.114624.

The *Chlamydia* effector IncE employs two short linear motifs to reprogram host vesicle trafficking

Khavong Pha[1], **Kathleen Mirrashidi**[1], **Jessica Sherry**[1], **Cuong Joseph Tran**[1], **Clara M. Herrera**[1], **Eleanor McMahon**[1], **Cherilyn A. Elwell**[1,*], **Joanne N. Engel**[1,2,3,*]

[1]Department of Medicine, University of California, San Francisco, San Francisco, CA 94143, USA

[2]Department of Microbiology and Immunology, University of California, San Francisco, San Francisco, CA 94143, USA

[3]Lead contact

SUMMARY

Chlamydia trachomatis, a leading cause of bacterial sexually transmitted infections, creates a specialized intracellular replicative niche by translocation and insertion of a diverse array of effectors (Incs [inclusion membrane proteins]) into the inclusion membrane. Here, we characterize IncE, a multifunctional Inc that encodes two non-overlapping short linear motifs (SLiMs) within its short cytosolic C terminus. The proximal SLiM, by mimicking just a small portion of an R-N-ethylmaleimide-sensitive factor adaptor protein receptor (SNARE) motif, binds and recruits syntaxin (STX)7- and STX12-containing vesicles to the inclusion. The distal SLiM mimics the sorting nexin (SNX)5 and SNX6 cargo binding site to recruit SNX6-containing vesicles to the inclusion. By simultaneously binding two distinct vesicle classes, IncE brings these vesicles in close apposition with each other at the inclusion to facilitate *C. trachomatis* intracellular development. Our work suggests that Incs may have evolved SLiMs to enable rapid evolution in a limited protein space to disrupt host cell processes.

In brief

Chlamydia trachomatis redirects host vesicular trafficking to survive intracellularly. Pha et al. demonstrate that the inclusion membrane protein IncE encodes two non-overlapping short linear motifs in its cytosolically exposed C terminus that simultaneously bring together STX7- and STX12-containing vesicles with SNX5- and SNX6-associated vesicles to facilitate inclusion fusion and progeny production.

*Correspondence: cherilyn.elwell@ucsf.edu (C.A.E.), jengel@medicine.ucsf.edu (J.N.E.).

AUTHOR CONTRIBUTIONS

Conceptualization, K.P., K.M., C.A.E., J.N.E., J.S., E.M., and C.M.H.; methodology, K.P., J.S., C.J.T., C.M.H., and E.M.; investigation, K.P., K.M., and C.J.T.; visualization, K.P., C.M.H., C.A.E., and J.N.E.; funding acquisition, J.N.E. and K.P.; supervision, K.P., C.A.E., and J.N.E.; writing – original draft, K.P., C.A.E., and J.N.E.; writing – review & editing, K.P., K.M., C.A.E., and J.N.E.

SUPPLEMENTAL INFORMATION

Supplemental information can be found online at https://doi.org/10.1016/j.celrep.2024.114624.

DECLARATION OF INTERESTS

The authors declare no competing interests.

Graphical abstract

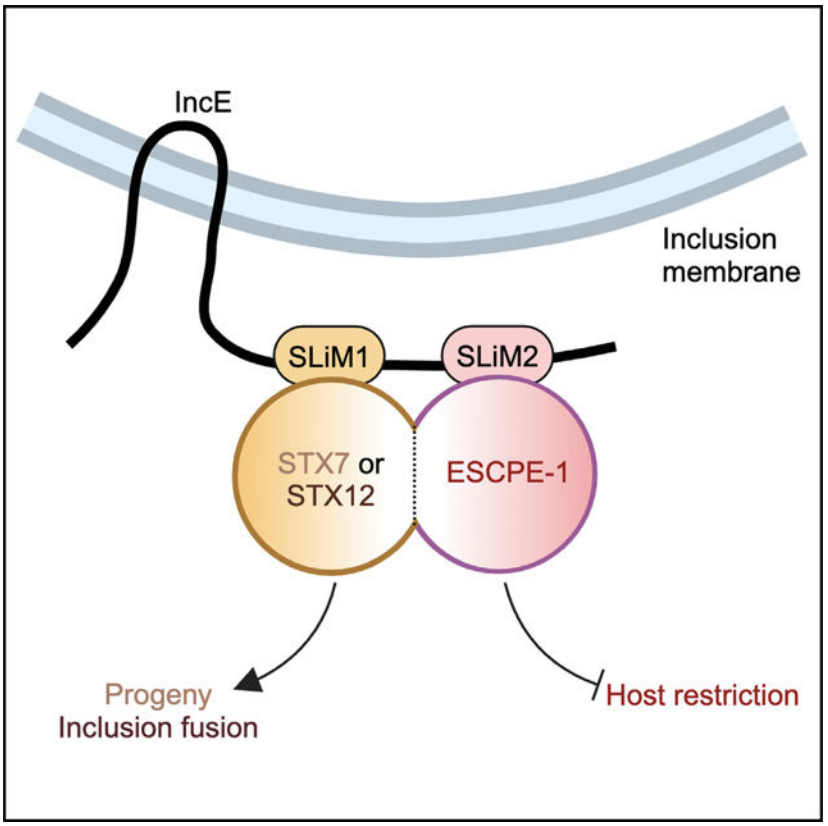

INTRODUCTION

Chlamydia trachomatis (*Ct*) infections are important causes of human disease for which no vaccine exists. Although infections can be treated with antibiotics, no drug is cost effective enough for widespread elimination of disease in developing nations.[1] This obligate intracellular parasite replicates within a privileged niche—a membrane-bound compartment termed the inclusion—where it subverts multiple host cell functions to survive.[2] *Chlamydiae* devotes up to 10% of its genome to a unique family of secreted effectors, the Incs (inclusion membrane proteins), which are translocated from the bacteria through the type III secretion system and inserted into the inclusion membrane.[3] These effectors are ideally positioned at the host-pathogen interface to function as scaffolds to mediate interactions between the inclusion and the host. We previously employed high-throughput affinity purification-mass spectroscopy (AP-MS) of human cells transfected with Incs to identify their host binding partners, with the goal of uncovering the function of Incs.[4] This analysis identified predicted high-confidence interactions between IncE, an early expressed Inc of unknown function, and proteins associated with two unrelated vesicle classes: (1) sorting nexin (SNX)5 and SNX6 and (2) syntaxin (STX)7 and STX12. SNX5 and SNX6, together with SNX1 and SNX2, comprise a subclass of retromer, the ESCPE-1 complex.[5] This multiprotein complex mediates retrograde-dependent recycling of cargo receptors from the endosome to the *trans*-Golgi network.[5,6] We and others solved the crystal structure of the IncE:SNX5 complex.[7–10]

We discovered that the C-terminal 24 amino acids of IncE bind with high affinity directly to a phylogenetically conserved hydrophobic groove in SNX5, which is also conserved in SNX6 homologs and the site at which cargo binds to SNX5 and SNX6.[5] Simultaneous depletion of SNX5 and SNX6 results in increased production of infectious progeny,[4,11] suggesting that the ESCPE-1 complex, or at least SNX5 and SNX6, functions as a restriction factor to limit *Ct* intracellular infection.

In this study, we explore the role of the predicted second class of IncE interactors, STX7 and STX12. STX7 and STX12 are closely related Q-N-ethylmaleimide-sensitive factor adaptor protein receptor (SNARE) proteins that mediate late and early endosome vesicle fusion, respectively,[12,13] but their role in *Ct* pathogenesis is unknown. Notably, neither STX7 nor STX12 has previously been associated with either SNX5/6 or the ESCPE-1 complex. STXs encode a 60–70 amino acid SNARE domain that can hetero-multimerize with other SNARE domains.[14,15] Typically, 1 R-SNARE associates with 3 Q-SNAREs, distributed between a donor membrane and a target membrane, along with Rab GTPases and the membrane tethering complex. Upon docking, the 4 SNARE domains align and form a stable 4 helix bundle (the *trans*-SNARE complex) to allow the "zippering" of the inner and outer leaflets of the donor and target membranes, leading to membrane fusion. A key feature of the SNARE domain is a highly conserved central ionic "0" layer that contains either a conserved arginine (R-SNARE) or glutamine (Q-SNARE). The salt bridges formed by the ionic layer, together with multiple hydrophobic interactions contributed by the flanking 7–8 leucine (heptad) repeats, nucleate the zippering that leads to membrane fusion.[16,17] Our studies reveal that IncE encodes a 6 amino acid short linear motif (SLiM) that mimics the −1 and 0 (ionic) layer of some R-SNAREs. We demonstrate that these 6 amino acids are required for IncE binding to STX7 and STX12, supporting a hypothesis that IncE binds to STX7 and STX12 through molecular mimicry. We found that STX7 and STX12 contribute to distinct steps in the *Ct* intracellular life cycle. IncE binding to STX7 is required for the production of infectious progeny, whereas IncE binding to STX12 facilitates homotypic inclusion fusion. Finally, we show that IncE binds to SNX5 or SNX6 and either STX7 or STX12 simultaneously. By tethering STX7/12- and SNX6-positive vesicles in close proximity to one another and the inclusion membrane, IncE may promote the creation of a nearby reservoir of accessible nutrients, proteins, and/or lipids that contribute to intracellular growth and survival.

RESULTS

IncE binds specifically to STX7 and STX12

Our interactome dataset identified STX7 and STX12 as high-confidence interactors with IncE.[4] We confirmed by transfection studies in HEK293T cells that endogenous STX7 and STX12 co-affinity purified (co-AP'd) with transfected $IncE_{Strep}$ but not with $IncG_{Strep}$, an unrelated Inc (Figure 1A). As a control for specificity, we immunoblotted for endogenous STX2, an unrelated STX that did not co-AP in our AP-MS dataset with transfected $IncE_{Strep}$,[4] and confirmed that it did not co-AP with transfected $IncE_{Strep}$. In HeLa cells infected with *Ct* strain LGV/L2 (L2) expressing $IncE_{FLAG}$ or $IncG_{FLAG}$ from a plasmid (L2+pIncE or L2+pIncG, respectively), STX7 and STX12, but not STX2, co-AP'd with

IncE but not with IncG (Figure 1B). Together, these results confirm a highly specific interaction between IncE and STX7 and STX12 in two different cell lines and both in the context of transfection and infection.

IncE binds STX7 and STX12 by mimicking a short motif found in the −1 and 0 (ionic) layer of an R-SNARE domain

STX7 and STX12 are Q-SNAREs that are more closely related to each other than to other Q-SNAREs (Figure S1), suggesting that IncE might bind to a region common to STX7 and STX12. To investigate the regions of STX7 and STX12 that are necessary for binding to IncE and delineate the region of IncE required for binding to STX7 and STX12, we constructed truncation mutants of STX7, STX12, and IncE (Figures 2A–2C, and 2D) and tested their ability to co-AP upon co-transfection. This analysis revealed that the SNARE and transmembrane (TM) regions of STX7 or STX12 are required for binding to IncE (Figures 2A–2D). For IncE, amino acids 37–100 are necessary and sufficient for the interaction with endogenous STX7 and STX12 (Figures 2E and 2F). We note that the STX7/12 binding region of IncE is distinct from its previously defined SNX5/6 binding region (Figure S2A).[7–10]

We further refined the region of IncE required for STX7/12 binding. As residues 37–100 encompass both TM domains (Figures 2E and S2B), we considered that the residues C-terminal to the second TM domain might encode the key STX7/12 interacting residues. Indeed, we identified a 6 amino acid sequence (VLENHG) that is homologous to the −1 and 0 (ionic) layer regions of two R-SNAREs, human VAMP3 (VLERDQ) and mouse VAMP5 (VLERHG) (Figure S2C). This 6 amino acid sequence is conserved, albeit with some variation, in IncE homologs (Figure S2C), suggesting that it is important for IncE function. We hypothesized that this region of IncE may mimic an R-SNARE motif to bind to the STX7 and STX12 Q-SNAREs.

To directly address the role of the IncE VLENHG sequence (hereafter referred to as the STX binding motif [StxBM]), we changed these 6 residues to alanine ($IncE_{\Delta StxBM}$) (Figure S2D) and tested the ability of this IncE variant to co-AP endogenous STX7 and STX12 in transfection and infection studies. We also created an IncE mutant in which residues V114 and F116 are changed to asparagine and aspartic acid, respectively (Figure S3D). This variant is predicted to be defective for IncE binding to SNX5 and SNX6[4] and termed $IncE_{\Delta SnxBM}$.

In transfection experiments, $IncE_{\Delta StxBM}$ no longer co-AP'd STX7 and STX12 but retained the ability to co-AP SNX5 and SNX6 (Figure S2E). Conversely, $IncE_{\Delta SnxBM}$ failed to co-AP SNX5 and SX6 but still co-AP'd STX7 and STX12 (Figure S2E). Thus, the SnxBM and StxBM each function independently to bind SNX5/6 or STX7/12, respectively.

To interrogate the role of the IncE StxBM and SnxBM in the context of infection, we generated a non-polar *incE* mutant strain (L2Δ*incE*) and complemented it with the following plasmids encoding anhydrous tetracycline (aTC)-inducible FLAG-tagged IncE variants: wild-type (WT) IncE, $IncE_{\Delta StxBM}$, $IncE_{\Delta SnxBM}$, or $IncE_{\Delta StxBM/\Delta SnxBM}$ (see Figure S3 for strain construction and characterization of L2Δ*incE*). We further characterized the

complemented strains as follows. We observed by FLAG immunoblot analysis that the IncE variants are all expressed at approximately similar levels to one another when induced with 2 ng/mL aTC (Figure S4A). When analyzed with an IncE antibody (which only recognizes IncE and $IncE_{\Delta StxBM}$ but not $IncE_{\Delta SnxBM}$ or $IncE_{\Delta StxBM/\Delta SnxBM}$), the protein levels of the ectopically expressed FLAG-tagged IncE or $IncE_{\Delta StxBM}$ are lower than endogenous IncE (Figure S4A). Thus, the plasmid-expressed IncE variants are not overexpressed compared to endogenous IncE. Finally, we confirmed by immunofluorescence microscopy that all IncE variants are localized to the inclusion membrane (Figure S4B).

We next examined the SNX and STX binding activity of each of the $IncE_{FLAG}$ variants in the context of infection. As expected, WT IncE co-AP'd with STX7, STX12, SNX5, and SNX6 (Figures 3A and 3B). $IncE_{\Delta StxBM}$ was unable to bind STX7 or STX12 during infection (Figures 3A and 3B), but SNX5 and SNX6 still co-AP'd with $IncE_{\Delta StxBM}$ (Figures 3A and 3B). Conversely, $IncE_{\Delta SnxBM}$ was unable to bind SNX5 and SNX6 during infection, whereas STX7 and STX12 still co-AP'd with this IncE variant (Figures 3A and 3B). Finally, STX7, STX12, SNX5, and SNX6 did not co-AP with $IncE_{\Delta StxBM/\Delta SnxBM}$ (Figures 3A and 3B). We conclude that during infection, the IncE StxBM is required for binding to STX7 and STX12 but not to SNX5 or SNX6. Conversely, the IncE SnxBM is required for binding to SNX5 and SNX6 but not to STX7 or STX12. These results further underscore that the StxBM is distinct and separate from the IncE SnxBM and that these two motifs function independently (Figure S2A).

IncE binding to STX7 and STX12 is required for late steps of infection

We tested the role of IncE binding to STX7 and STX12 in the *Ct* intracellular life cycle. Quantitation of *Ct* inclusion formation, specifically the number, size, and localization of inclusions, is a robust metric for early steps in the infection process. Quantification of progeny production additionally assesses late steps in infection (Figure S5A).

We first quantified the inclusion formation and production of infectious progeny by an inter-strain comparison of WT (L2+vector) to the *incE* mutant (L2Δ*incE*+vector). Surprisingly, no differences were observed between WT and the *incE* mutant in inclusion formation, inclusion size, or production of infectious progeny (Figures S5B–S5D). As depletion of SNX5 and SNX6 enhances progeny production,[4,11] we considered that if STX7 and/or STX12 are required for progeny production, then the *incE* deletion mutant might exhibit no change in production of infectious progeny compared to WT. With this rationale in mind, we compared progeny production when cells were infected with the individual complemented L2Δ*incE* strains. As the variants are under the control of an aTC-inducible promoter, we performed intra-strain comparisons in the presence or absence of an inducer and demonstrate that the IncE variants are induced near equivalently (Figure S4A). This strategy has the important advantage that it bypasses the requirement that infection of different strains be performed at an equal multiplicity of infection (MOI), although similar MOIs were used for each strain. Remarkably, only L2Δ*incE*+p$IncE_{\Delta StxBM}$, the IncE variant that cannot bind STX7/12 but retains binding to SNX5/6, exhibited decreased production of infectious progeny (Figure 4B). As well, there was a trend toward decreased inclusion formation in this strain, although it did not reach statistical significance (Figure 4A).

Together, these studies reveal a critical role for IncE binding to STX7/12 during intracellular infection that is only unmasked when IncE is still able to bind to SNX5/6 but not to STX7/12.

IncE binding to STX7 and STX12 is required for inclusion fusion

The experiments described above were performed at an MOI of ~1, conditions under which most cells are infected with a single elementary body (EB) and therefore initiate infection with only a single inclusion. An important aspect of *Ct* development is the ability of multiple inclusions within a single cell to fuse with each other (inclusion fusion), which occurs when cells are infected at a high MOI.[19] Under these conditions, which can be observed in *Ct* human infections,[20,21] individual EBs are initially taken up into separate inclusions that subsequently undergo homotypic fusion commencing at ~12 h post-infection (hpi).[19] Inclusion fusion is thought to be important in the pathogenesis of *Ct* infections *in vivo*. Human genital tract infections with naturally occurring *Ct* variants that fail to undergo fusion due to loss of the inclusion protein IncA exhibit milder pathology.[21,22] Likewise, in a mouse genital tract infection model, L2D*incA* shows decreased colonization.[23]

To assess the role of IncE in inclusion fusion, we infected HeLa cells at a high MOI. An increase in the average number of inclusions per field relative to L2+vector indicates a defect in inclusion fusion (Figures S6A and S4C). As a control, we included a mutant that lacks IncA (L2Δ*incA*), which is indispensable for inclusion fusion.[24,25] *ΔincE* exhibited an increase in the number of inclusions compared to L2+vector at 24 hpi (Figures 4C and S6A). Strains lacking functional IncE or expressing IncE lacking both the SnxBM and StxBM (L2Δ*incE*+pVector and L2*ΔincE*+pIncE$_{\Delta StxBM/\Delta SnxBM}$) exhibited decreased inclusion fusion at 24 hpi (Figures 4C and S6A).

To delineate whether the SnxBM or StxBM (or both) was required for efficient inclusion fusion, we quantified fusion at 24 and 48 hpi in cells infected with the *incE* mutant that cannot bind STX7/STX12 (L2*ΔincE*+pIncE$_{\Delta StxBM}$) and in cells infected with the *incE* mutant that cannot bind SNX5/SNX6 (L2*ΔincE*+pIncE$_{\Delta SnxBM}$). Inclusion fusion was not restored upon expression of pIncE$_{\Delta StxBM}$ at 24 hpi, whereas it was restored upon expression of pIncE$_{DSnBM}$ at 24 hpi (Figures 4C and S6A).

Finally, we compared inclusion fusion of all of the IncE variants to inclusion fusion in L2 and to *ΔincA* at 48 hpi. Whereas inclusion fusion in *ΔincA* was still defective at 48 hpi, the IncE variants lacking the StxBM exhibited similar levels of inclusion fusion compared to L2 by 48 hpi (Figure S6B). We conclude that IncE binding to STX7/12 contributes to efficient inclusion fusion, whereas binding to SNX5/6 is not required.

STX7 and STX12 play distinct roles in *Ct* infection

Ct expressing the IncE variant that cannot bind STX7/12 exhibits two different phenotypes —a decrease in progeny production and a delay in inclusion fusion. These two phenotypes are independent, as the *ΔincA* mutant, which fails to undergo inclusion fusion, does not exhibit a progeny defect during infection in cultured cells.[25] Thus, STX7 and STX12 could play distinct roles in *Ct* infection—binding to one STX may be required for efficient inclusion fusion, whereas binding to the other STX may be required for progeny production.

To test this hypothesis, cells were depleted for STX7 or STX12 by RNAi, infected with L2, and assayed for inclusion formation and production of infectious progeny. Depletion of STX7 (which did not affect STX12 levels; Figures S7A and S7B) resulted in a decrease in progeny production (Figure 5A) but had no effect on inclusion formation or inclusion fusion (Figures 5B–5D). In contrast, depletion of STX12 (which did not affect STX7 levels; Figures S7A and S7B) resulted in a defect in inclusion fusion at 24 hpi (Figures 5B–5D) but had no statistically significant effect on progeny production (Figure 5A). Depletion of SNX5/6 had no effect on inclusion fusion (Figures 5C and 5D). Together, these results support the hypothesis that binding of IncE to STX7 and STX12 contributes to distinct and separate aspects of *Ct* development. STX7 is required for efficient progeny production, while STX12 is required for efficient inclusion fusion. These experiments provide additional support for the observation that a decrease in inclusion fusion does not affect the production of infectious progeny.

IncE interacts simultaneously with STX7/12 and SNX5/6 to tether together distinct vesicle classes at the inclusion

The remarkable compactness of the IncE C terminus, with 42 amino acids encoding two non-overlapping motifs that interact with proteins associated with distinct classes of vesicles, raised the possibility that such a reductionist architecture enables simultaneous and synergistic interactions of IncE with SNX5 or SNX6 and STX7 or STX12. To explore this notion, we determined whether IncE could simultaneously co-AP SNX5 or SNX6 with STX7 or STX12 in the context of infection. In the absence of infection, endogenous STX7 or STX12 did not co-AP with transfected $SNX5_{FLAG}$ or mCherry-SNX6 (Figures S8A and S8B), confirming that these SNAREs do not normally interact with SNX5 or SNX6. However, upon infection with L2, endogenous STX7 or STX12 co-AP'd with transfected $SNX5_{FLAG}$ or mCherry-SNX6 (Figures S8A and S8B). This interaction was IncE dependent, as no interaction was observed between $SNX5_{FLAG}$ or mCherry-SNX6 and STX7 or STX12 in the *incE* mutant (L2Δ*incE*). We conclude that IncE can interact simultaneously with SNX5 or SNX6 and STX7 or STX12.

We therefore investigated the potential biological consequence(s) of the ability of IncE to interact simultaneously with STX7 or STX12 and SNX5 or SNX6 at the inclusion membrane. SNX5 and SNX6 can be recruited to the inclusion membrane,[4] and SNX6 is present on vesicles near the inclusion membrane[4] (see also Figure S4). We examined whether STX7- and STX12-containing vesicles are recruited to the inclusion and whether these vesicles fuse with the inclusion. Using live-cell imaging of L2-infected cells, we observed GFP-STX7- and GFP-STX12-containing vesicles close to and sometimes fusing with the inclusion membrane (Videos S1 and S2), although these fusion events appeared to be infrequent.

We also considered that simultaneous binding of IncE to STX7 or STX12 and SNX5 or SNX6 could tether together two normally distinct classes of vesicles in close proximity to one another at the inclusion. As this redirection of vesicular trafficking would be IncE dependent and IncE is restricted to the inclusion membrane, we predict that STX7/12 and SNX5/6 vesicles in close apposition would be observed proximal to, but not distal to, the

inclusion. To test this hypothesis, we examined whether GFP-STX7 and/or mCh-STX12 overlapped with endogenous SNX6 in vesicles that were either proximal or distal to the inclusion. For this quantitation, we determined the relative location of the maximum fluorescence intensity of each of the 3 proteins with respect to each other in 30 vesicles proximal to (within 1 μm) and 30 vesicles distal to (>5 μm) the inclusion for each experimental group (Figure 6A).

In vesicles distal to the inclusion, the maximum fluorescence intensity of GFP-STX7 and mCh-STX12 was distinct from and did not overlap with endogenous SNX6 (Figures 6A and 6B). The average maximum fluorescence intensity of GFP-STX7 or mCh-STX12 was displaced 0.26 and 0.29 μm from the maximum fluorescence intensity of SNX6, respectively (Figure 6B; Table S1), which is greater than the average diameter of endosomal vesicles.[26] Importantly, in vesicles proximal to the inclusion, the maximum fluorescence intensity of GFP-STX7 and mChSTX12 was significantly less displaced from endogenous SNX6, <0.06 μm (Figures 6B and 6C; Table S1). For reference, the maximum fluorescence intensity of GFP-STX7 and mChSTX12 often overlapped with one another, in vesicles both proximal and distal to the inclusion (Table S1). This result is not entirely unexpected since both STX7 and STX12 are reported to localize to endosomes, although STX7 may localize to late endosomes,[27] while STX12 may localize to early endosomes.[28] Altogether, these experiments suggest that IncE serves as a bifunctional tether to bring together SNX6-containing vesicles with STX7- and STX12-containing vesicles.

We tested this prediction explicitly by quantitating the overlap of GFP-STX7, mCherry-STX12, and endogenous SNX6 in vesicles proximal and distal to inclusions in cells infected with L2Δ*incE*. Indeed, the overlap of STX7 or STX12 with SNX6 in vesicles proximal to the inclusion was abrogated in the *incE* mutant, increasing from 0.03 to 0.045–0.15 and 0.2 μm, respectively. Importantly, there was minimal change in the overlap of STX7 with STX12 in cells infected with L2 expressing or lacking IncE (Table S1). The overlap of STX7 or STX12 with SNX6 was restored when the *ΔincE* mutant was complemented with WT IncE (0.051 and 0.057 μm, respectively; Figure 6C; Table S1). Similar to infection with L2, there was greater displacement of STX7 or STX12 from SNX6 in vesicles distal to the inclusion (Figure 6A; Table S1): 0.375 or 0.360 μm, respectively. In cells infected with L2Δ*incE* expressing either the single or double IncE mutants ($IncE_{\Delta StxBM}$, $IncE_{\Delta SnxBM}$, $IncE_{\Delta StxBM/\Delta SnxBM}$), the displacement of STX7 or STX12 from SNX6 was similar to that observed in the *ΔincE* mutant in inclusion-proximal vesicles (Figure 6C; Table S1). We do note that the displacement of STX7 or STX12 from SNX6 was somewhat greater in $IncE_{\Delta SnxBM}$ than $IncE_{\Delta StxBM}$ for unclear reasons (Table S1). We conclude that IncE, through its StxBM and SnxBM domains, promotes the recruitment of STX7/12- and SNX6-positive vesicles in close proximity to each other at the *Ct* inclusion membrane.

DISCUSSION

In this work, we demonstrate that IncE is a remarkably compact scaffold that simultaneously interacts with numerous host vesicle-associated proteins to facilitate its intracellular growth and development. We and others have previously shown that SNX5 and SNX6 are recruited to the inclusion by binding to a short motif (the SnxBM) present in the C terminus of

IncE. In doing so, IncE displaces native SNX5/6 cargo, such as the mannose-6-phosphate receptor,[4,7,10] providing a more permissive environment for late steps in the *Ct* intracellular life cycle (Figure 7). Here, we reveal that IncE encodes a separate non-overlapping 6 amino acid motif (the StxBM) upstream of the SnxBM that mimics the −1 and 0 (ionic) layer of R-SNAREs. The StxBM enables IncE to bind to a subset of Q-SNAREs, STX7 and STX12, during infection. Importantly, we demonstrate that the IncE:STX interactions contribute to distinct steps in the intracellular life cycle: intracellular growth and progeny production (STX7) and homotypic inclusion fusion (STX12).

By comparing the absolute distance between endogenous SNX6, transfected STX7, and transfected STX12, we demonstrate that IncE, by binding simultaneously to STX7 or STX12 and SNX6, recruits and brings together vesicles that harbor STX7, STX12, and SNX6. Importantly, STX7 and STX12 do not co-localize with SNX6 in the absence of IncE or in vesicles distant from the inclusion. While we expect that SNX5 would exhibit similarly closer localization to STX7 and STX12 in an IncE-dependent manner, the absence of an antibody that recognizes endogenous SNX5 precluded testing this prediction directly. Our results suggest that IncE functions in an inclusion-autonomous manner, as would be expected for a membrane-bound effector.

Several possible models could account for the IncE-dependent altered relative localization of STX7 or STX12 with SNX6 (and by inference, SNX5). Vesicles close to the inclusion could be smaller than vesicles distal to the inclusion, allowing STX7/STX12 to measure closer to SNX6, but one would have to postulate that this is an IncE-dependent process. Alternatively, IncE may tether these two classes of vesicles in close proximity to each other. Indeed, by tethering these vesicles in close apposition, IncE could promote their fusion with each other to form a hybrid vesicle. Further studies utilizing higher-resolution microscopy and/or time-lapse immunofluorescence microscopy will be required to test this notion. Notably, the measured distance of STX7 or STX12 from SNX6 was often less than the average published diameter of endosomal vesicles (reported to be 0.1–0.5 μm[26]), consistent with hybrid vesicle formation.

It is intriguing that VAMP3 and VAMP8, which are cognate R-SNAREs for STX7 and STX12,[29–32] are recruited to the inclusion[11] and also co-AP with IncE following transfection.[4] VAMP3 has been associated with retromer-dependent transport of the mannose-6-phosphate receptor,[33] a well-characterized cargo of the ESCPE-1 complex.[34] We speculate that VAMP3 and VAMP8 could cooperate with the StxBM on IncE to promote fusion of the STX7/STX12 vesicles with SNX6 (and presumably SNX5)-containing vesicles.

We suggest that IncE, by promoting the tethering of normally distinct vesicle classes at or near the inclusion, could create a nearby reservoir of accessible nutrients, proteins, and/or lipids that contribute to intracellular growth and homotypic inclusion fusion. STX12 has been implicated in cholesterol transport.[35] Although *Ct* requires cholesterol for intracellular growth and development,[36] the role for cholesterol in inclusion fusion remains to be explored. Future studies will focus on determining the nature of the STX7/12- and SNX5/6-containing vesicles, whether they undergo fusion with each other, the identity of the host

constituents contributed by these vesicles, and the potential crosstalk between the SNXs and STXs.

It is currently unclear why the loss of IncE has no apparent effect on inclusion formation or progeny production, while an IncE mutant defective in binding to STX7 and STX12 exhibits a mild inclusion defect and a statistically significant progeny defect. One possibility is that IncE binding to STX7/12 is required for progeny production, whereas its binding to SNX5/6 restricts progeny production. If the $IncE_{\Delta StxBM}$ mutant can bind more efficiently to SNX5/6, then this scenario would explain our observation.

Our work reveals that IncE encodes two SLiMs in its short C-terminal tail. SLiMs are composed of 3–15 amino acids, often embedded in intrinsically disordered or coiled-coil regions. SLiMs typically adopt a more structured conformation that serves as a binding interface to a structured (globular) partner.[37] The human proteome is estimated to encode millions of SLiMs.[38] SLiMs are also found in viral proteins[39,40] and occasionally in bacterial effectors.[41] The importance of the two SLiMs encoded in IncE is highlighted by the fact that the VLE (found in the StxBM) and VQF (found in the SnxBM) motifs are conserved, albeit with some variation, in several of the IncE homologs found in multiple *Chlamydia* species (Figure S3C). We also note that the arginine in the 0 layer of the R-SNARE is changed to an asparagine (L2), an aspartic acid (serovars D and B), or a histidine (*C. muridarum* and *C. suis*). How this impacts IncE binding to STX7 or STX12 is unclear; some substitutions for the conserved arginine have been reported to still be functional for SNARE-mediated fusion.[42]

The use of SLiMs by Incs to encode a protein-protein binding surface empowers these inclusion-anchored proteins to disrupt, relocate, or bring together new combinations of protein. Remarkably, IncE accomplishes all 3 of these tasks: (1) the SnxBM disrupts SNX5/6 binding to the mannose-6-phosphate receptor and possibly to other SNX5/6 cargo,[7] (2) both the SnxBM and StxBM recruit vesicles to the inclusion, and (3) by recruiting these 2 distinct classes of vesicles simultaneously, IncE potentially facilitates the formation of a new hybrid class of vesicles.

We anticipate that the use of SLiMs will be a recurring theme in Inc biology and suggest that SLiMs could account for several unique aspects of this obligate intracellular pathogen. Recently, several Incs have been reported to encode their host protein binding interfaces within a short unstructured region or coiled-coiled sequences in their cytosolically exposed C termini.[7,43,44] As Incs are rapidly evolving,[45] the use of SLiMs would allow for the rapid diversification of Inc-encoded protein binding domains. Indeed, SLiMs are predicted to evolve rapidly *ex nihilo* since they require only a few key amino acids to create a binding surface.[46,47]

Altogether, these results reveal that the C terminus of IncE is an extraordinarily compact multitasker. This one Inc illustrates the vast potential of the many other *Chlamydia* Incs to modulate and even reprogram the hostile intracellular environment of the host into a milieu that is conducive for the success of this obligate intracellular pathogen. These studies

exemplify the power of mining the *Ct*-host interactome for new insights into both pathogen virulence strategies and host cell biology.

Limitations of the study

A potential caveat of this study is that our immunofluorescence data and analysis of STX7 and STX12 localization during infection utilize transfected fluorescently tagged STX7 and STX12 proteins, as antibodies that recognize endogenous STX7 or STX12 in immunofluorescent studies are not commercially available. Likewise, due to the absence of a commercially available antibody that recognizes SNX5 for immunofluorescent studies, we were not able to compute the distance between SNX5 and either STX7 or STX12.

STAR★METHODS

RESOURCE AVAILABILITY

Lead contact: Further information and requests for resources and reagents should be directed to and will be fulfilled by the lead contact, Joanne Engel (jengel@medicine.ucsf.edu).

Materials availability: All unique/stable reagents generated in this study are available from the lead contact upon request, but we may require reasonable compensation by the requestor for processing and shipping charges.

Data and code availability

- Data reported are available upon request.
- All custom codes are included as a supplemental item in this paper.
- Any additional information required to reanalyze the data reported in this work paper is available from the lead contact upon request.

METHOD DETAILS

Cell culture and bacterial propagation: HeLa and Vero cells were obtained from American Type Culture Collection (ATCC). HeLa cells were cultured and maintained in Eagle's Minimum Essential Medium (MEM; University of California, San Francisco Cell Culture Facility) supplemented with 10% (v/v) fetal bovine serum (FBS) from Gemini at 37°C in 5% CO_2. HEK293T cells were a generous gift from Nevan Krogan (University of California, San Francisco). HEK293T and Vero cells were cultured and maintained in Dulbecco's modified Eagle's Medium (DMEM, UCSF Cell Culture Facility) supplemented with 10% (v/v) FBS at 37°C in 5% CO_2. Cells were routinely tested for mycoplasma (Sigma). *C. trachomatis* L2 (434/Bu; hereafter referred to as L2) was a generous gift from Deborah Dean (University of California, San Francisco). L2 and derivative strains used in these studies are listed under "experimental models: organisms/strains" in the key resources table. L2 was routinely propagated in Vero cell monolayers as previously described.[57] HeLa cells were used for all infection studies, and HEK293T cells were used for all ectopic expression experiments. Stellar chemically competent *Escherichia coli* (Takara Bio) were used to propagate constructs for ectopic expression in mammalian cells, while 10-beta *E.*

coli (NEB) and *dam*$^{-}$/*dcm*$^{-}$ chemically competent *E. coli* (NEB) was used to propagate constructs for transformation into L2.

Antibodies and reagents: Primary antibodies were obtained from the following sources: mouse anti-STX7 (Santa Cruz Biotechnology Inc, sc-514157), rabbit anti-STX12 (Atlas Antibodies, HPA055300), rabbit anti-STX2 (Abcam, AB12369–1001), rabbit anti-SNX5 (Proteintech, 17918–1-AP), mouse anti-SNX6 (Santa Cruz Biotechnology Inc, sc-365965), goat anti-SNX6 (Santa Cruz Biotechnology, sc-8679), mouse anti-FLAG (Sigma, F3165), rabbit anti-FLAG (Sigma, F7425), mouse anti-GAPDH (Millipore, MAB374), goat anti-MOMP L2 (Fitzgerald, 20C-CR2104GP), rabbit anti-Strep TagII HRP (Millipore, 71591–3), mouse anti-GFP (Roche, 11814460001), mouse anti-HSP60 (Santa Cruz Biotechnology Inc, sc57840), and rabbit anti-RFP (Rockland, 600-401-379-RTU). Mouse anti-IncA and rabbit anti-IncG antibodies were kindly provided by Dan Rockey (Oregon State University) and Ted Hackstadt (Rocky Mountain Laboratories), respectively. Rabbit anti-IncE antibody generated against the peptide CKSSPANEPAVNFFKGKNGS (corresponding to amino acids 102–121) was kindly provided by Ted Hackstadt or prepared commercially by Genscript. Secondary antibodies for immunofluorescence were derived from donkey and purchased from Life Technologies: anti-goat Alexa Fluor 647, anti-mouse Alexa Fluor 647, anti-mouse Alexa Fluor 568, anti-rabbit Alexa Fluor 568, anti-goat Alexa Fluor 488, anti-rabbit Alexa Fluor 488, anti-mouse Alexa Fluor 405. Heparin sodium salt was purchased from Sigma (H3393). Primers (listed in the oligonucleotides section of the key resources table) were commercially generated by Integrated DNA Technologies or by Elim Biopharm. Dilutions of primary antibodies for immunoblotting and immunofluorescence were performed as follow: anti-Strep (1:1,1000), anti-FLAG (1:3,000 and 1:200), anti-GFP (1:3,000), anti-RFP (1:3,000), anti-STX7 (1:1,000), anti-STX12 (1:1,000), anti-STX2 (1:1000), anti-SNX5 (1:1,000), anti-SNX6 (1:1,1000), anti-GAPDH (1:20,000), anti-MOMP (1:5,000 and 1:500), anti-IncE (1:500 and 1:100), anti-IncG (1:500 and 1:100), and anti-IncA (1:500 and 1:100).

Plasmid construction: The IncG gene, IncE gene and IncE deletion constructs used for ectopic expression studies were PCR amplified from purified genomic L2 DNA and subcloned into the EcoRI and NotI sites in pcDNA4.0/2xStrepII.[54] To generate the IncE point mutants used for ectopic expression studies, primers harboring point mutations were used to PCR amplify IncE DNA fragments containing the indicated point mutations. The IncE DNA fragments were ligated together by overlapping PCR and IncE mutants were subcloned into the EcoRI and NotI sites in pcDNA4.0/2xStrepII. STX7 and STX12, and various deletion derivatives were PCR amplified from STX7 and STX12 plasmids (a kind gift of Dr. Sourav Bandyopadhyay, University of California, San Francisco)[55] and subcloned into the HindIII and KpnI sites in pEGFP C1 and pmCherry C1 vectors. To generate pSUmC-*incE-loxP-aadA-gfp*, 3kb DNA fragments from up- and downstream of *incE* were PCR amplified separately from genomic L2 DNA and subcloned into the SalI and SbfI sites, respectively, in pSUmC-*loxP-aadA-gfp* (a kind gift of Dr. Kenneth Fields, University of Kentucky)[53] by Gibson assembly. The *E. coli/Chlamydia* shuttle vector p2TK2-mCherry (a kind gift of Dr. Isabelle Derre, University of Virginia)[52] was modified by removing the *mcherry* gene by InFusion cloning to generate p2TK2. For plasmids that were transformed into L2 strains, IncE variants were PCR amplified from the corresponding IncE-encoding

plasmid and cloned into EagI and SbfI sites in the p2TK2. All cloning were verified by forward and reverse sequencing.

Affinity purifications (APs): For StrepTactin APs, 6×10^6 HEK293T cells were seeded in each of two to three 10 cm^2 plates. Cells were transfected using Continuum Transfection Reagent (GeminiBio), following the manufacturer's instructions. At 24 h post transfection, cells were scraped in PBS, pelleted, lysed in 1 mL of ice-cold Lysis Buffer (50 mM Tris pH 7.4, 150 mM NaCl, 1 mM EDTA, 0.5% Igepal (Sigma)) at 4°C for 20 min while rotating, and centrifuged at 14,000 RPM at 4°C for 20 min. Lysates were incubated with 60 μL of Strep-Tactin Sepharose beads (IBA) overnight on a nutator. Beads were washed five times in 1mL Lysis Buffer containing 0.5% Igepal. Samples were eluted in 60 μL of 2.5mM D-desthiobiotin (IBA) in Lysis Buffer for 30 min on rocker at room temperature. Eluates were immunoblotted with anti-STX7, anti-STX12, anti-STX2, anti-SNX5, anti-SNX6, anti-Strep-HRP, and anti-GAPDH antibodies.

For other APs, HeLa cells (3×10^5 cells) were seeded in each well of two 6-well plates. Cells were transfected with indicated construct using Continuum Transfection Reagent (GeminiBio) according to the manufacturer's instructions. At 6–24 h post transfection, HeLa cells were infected with the indicated L2 strains (MOI ~3) by centrifugation at 1000 RPM for 30 min at 4°C. Infected cells were incubated at 37°C in 5% CO_2 for 30 min, and infection media was removed. Fresh media containing 50 ng/mL anhydrous tetracycline (aTC, Takara biotech) was added to infected cells. At 24 h post infection (hpi), cells were scraped in PBS, pelleted, and lysed in 1 mL of ice-cold Lysis Buffer containing 0.5% Igepal at 4°C for 20 min while rotating. Lysates were centrifuged at 14,000 RPM at 4°C for 20 min. For FLAG APs, lysates were incubated with 60 μL of anti-FLAG M2 Magnetic Beads (Sigma) overnight on the nutator. Beads were washed five times in 1mL Lysis Buffer containing 0.5% Igepal. Samples were eluted with 150 μg FLAG peptide (Sigma) in Lysis Buffer for 30 min on a rocker at room temperature. For mCherry and GFP APs, lysates were incubated with 10 μg rabbit anti-RFP and mouse anti-GFP antibodies, respectively, overnight on the nutator. Lysates were then incubated with Protein G Agarose beads (Pierce) on the nutator at 4°C for 3 h. Beads were washed five times in 1mL Lysis Buffer. Samples were eluted with 3X LDS Sample Buffer. Eluates were immunoblotted with anti-STX7, anti-STX12, anti-STX2, anti-SNX5, anti-SNX6, anti-Strep-HRP, anti-RFP, anti-GFP, anti-MOMP, and anti-GAPDH antibodies.

siRNA depletion studies: HeLa cells were transfected with SmartPool siRNA (Dharmacon) for STX7, STX12, SNX5 and SNX6, or siGENOME pool non-targeting #2 using Dharmafect following the manufacturer's instructions (Dharmacon). At 72 h post transfection, cells were infected with L2 (MOI ~0.8 or ~5) by centrifugation at 1000 RPM for 30 min at 4°C followed by incubation at 37°C in 5% CO_2 for 30 min. Infection media was removed, and fresh media was added to infected cells. At 24 hpi and 48 hpi, infected cells were processed for quantitation of inclusion formation or production of infectious progeny, respectively, as described below. siRNA depletion efficiency was determined by immunoblotting lysates with anti-STX7, anti-STX12, anti-SNX5, anti-SNX6, and anti-GAPDH antibodies.

Fluorescence microscopy: HeLa cells were grown on acid-treated glass coverslips (Warner Instruments) in 24-well plates. For localization of $IncE_{FLAG}$ variants, cells were transfected with GFP-SNX6 using Effectene (Qiagen) following manufacturer's instructions. For experiments assessing co-localization of STX7, STX12, and SNX6 vesicles, cells were co-transfected with GFP-STX7 and mCherry-STX12 as described above. At 6–24 h after transfection, cells were infected with indicated L2 strains. Bacteria suspended in MEM supplemented with 10% FBS were centrifuged onto cell monolayers at 1000 RPM for 30 min at 4°C. Infected cells were incubated at 37°C in 5% CO2 for 1 h. Infection media were aspirated, fresh media containing 2 ng/mL aTC were added, and cells were incubated at 37°C in 5% CO2 for 24 h or 48 h. Infections for experiments to assay protein localization were performed at MOI ~1 in the presence of 2 ng/mL aTC. Experiments assaying homotypic inclusion fusion were performed at MOI ~5 in the presence or absence of 2 ng/ml aTC. Experiments assaying inclusion formation were performed at MOI ~1 in the presence or absence of 2 ng/mL aTC. For experiments assaying production of infectious progeny, EBs were harvested from primary infections (as described below) performed at MOI ~1 in the presence or absence of 2 ng/mL aTC. The harvested EBs were then used to infect fresh HeLa cells at varying MOIs on coverslips. At 24 hpi, the cells were fixed in 4% PFA in PBS for 15 min at room temperature and then permeabilized in 0.1% Triton X-100 in PBS for 15 min at room temperature. Cells were blocked in PBS containing 1% BSA for 1 h and then stained with indicated primary and fluorophore-conjugated secondary antibodies in 1% BSA for 1 h each. Coverslips were mounted on Vectashield mounting media with or without DAPI (Vector Laboratories) and imaged on laser scanning disc confocal microscope.

For live cell microscopy, HeLa cells were grown on 24-well glass-bottom plates (MatTek, P24G-1.0–13-F) and co-transfected mCherry-SNX5 as well as either GFP-STX7 or GFP-STX12 using Continuum Transfection Reagent (GeminiBio), following manufacturer's instructions. At 6 h after transfection, cells were infected with L2 (MOI ~1). At 24 hpi, cells were washed with pre-warmed PBS. Phenol-free DMEM supplemented with 10% FBS and 1mM HEPES (University of California, San Francisco Cell Culture Facility) were added and infected cells were imaged on spinning disk confocal microscope as described below.

Images were acquired using Yokogawa CSU-X1 spinning disk confocal mounted on a Nikon Eclipse Ti inverted microscope equipped with an Andora Clara digital camera and CFI APO TIRF 60X oil or PLAN APO 40x objective. Single Z slices were acquired for images used for protein localization, quantifying inclusion formation, inclusion size, production of infectious progeny, and homotypic inclusion fusion. For images used for assessing vesicle co-localization, 0.3 μm-thick z stack images were acquired. For live cell imaging, single Z slices were acquired for 60 s at 1 frame per second using the CFI APO TIRF 60X oil objective lens. Images were acquired by NIS-Elements software 4.10 (Nikon). For each set of experiments, the exposure time for each filter set for all images was identical. Images were processed with FIJI Software to quantify inclusion numbers and sizes.

Generation of L2 strains: L2 overexpressing $IncE_{FLAG}$ was generated as previously described.[58] 10 μg DNA was used to transform 1×10^7 infection forming units (IFUs) of L2 in 200 μl Transformation Buffer (10 mM Tris pH 7.4 in 50 mM CaCl2). Following 30 min incubation at room temperature, the transformation mix was added to 12 mL MEM

supplemented with 10% FBS. 2 mL of suspended bacteria was added to each well of 6-well plate containing Vero cells (2×10^5/well). At 12 hpi, 5 μg/mL Ampicillin (Amp; Sigma) and cycloheximide (1 μg/mL, Sigma) was added to select for transformed L2. After 3 initial passages, Amp was increased to 50 μg/mL and L2 transformants were passaged 2–3 times in Vero cells. Clonal populations of transformants were isolated under Amp selection by plaque assay in Vero cells. L2 overexpressing $IncG_{FLAG}$ was a generous gift from Dr. Isabelle Derre (University of Virginia).

Deletion of *incE* in L2 (hereafter referred to L2Δ*incE*) was generated using floxed-cassette allelic exchange mutagenesis.[53] L2 was transformed with unmethylated pSUmC-*incE*-*loxP*-*gfp*-*aadA* in Transformation Buffer as described above. At 12 hpi, Spectinomycin (Spec; 500 μg/mL, Sigma), aTC (50 ng/mL; Takara Bio), and cycloheximide (1 μg/mL) were added to select for transformed L2. After 3–4 initial passages, surviving transformants expressing GFP and mCherry were selected by passage in Vero cells in the presence of Spectinomycin (Spec, 500 μg/mL) but without aTC to enrich for plasmid integration by allelic exchange. Clonal populations harboring *incE*::loxP-*aadA*-*gfp* was plaque-purified in the presence of Spec (500 μg/mL) selection. After 2–3 passages in Vero cells, the plaque-purified transformants were transformed with pSU-CRE, which expresses Cre recombinase, to allow for excision of the *aadA*-*gfp* cassette on the chromosome. At 12 hpi, Ampicillin (Amp, 5 μg/mL) and aTC (50 ng/mL) were added to select for transformants. After 3–4 passages, transformants expressing only mCherry (*aadA*-*gfp* cassette excised) were passaged in the absence of Amp and aTC to allow for loss of pSU-CRE to generate L2Δ*incE*. Loss of *incE* by Cre-mediated excision at the lox sites was confirmed by PCR screening using a forward primer to the upstream gene (*incD*) and a reverse primer to the downstream gene (*incF*). The presence or absence of the transcripts encoded in the operon (IncD, IncE, IncF, IncG) were confirmed by (i) RT-PCR (primers are listed in the oligonucleotide section of the key resources table), performed according to the manufacturers protocol (Qiagen) (ii) immunoblot analysis, using antibodies to IncE and IncG, and (iii) immunofluorescence using primary antibodies to IncA, IncE, and IncG. L2Δ*incE* was transformed with p2TK2 (empty vector) or complemented with the indicated p2TK2-$IncE_{FLAG}$ ($IncE_{FLAG}$) variants. For protein expression, HeLa cells were infected as described above with indicated L2 strains (MOI ~5) in the presence of 2 ng/mL aTC for 24 h. Cell lysates were immunoblotted with anti-IncE, anti-FLAG, and anti-HSP60. L2Δ*incA*, carrying a *bla* cassette inserted at the *incA* locus, was generated using TargeTron.[24]

Bioinformatics: The full length IncE protein sequence from L2 were analyzed using to HMMTOP,[59] TMpred,[60] SOSUI,[61] and TMHMM[60] using standard parameters to predict the two transmembrane on IncE. Multiple sequence alignment of IncE homologs, Q-SNAREs, and R-SNAREs were performed using Clustal Omega.[62]

QUANTIFICATION AND STATISTICAL ANALYSIS

Quantitation of inclusion formation

To quantify inclusion formation, HeLa cells infected with the indicated L2 strains for 24 or 48 h were fixed with 4% PFA, stained with anti-MOMP and fluorescent secondary

antibodies, and visualized by spinning disk confocal microscopy. A total of 11 fields per coverslip x 3 (technical replicates) were acquired for a total of 33 fields per condition. Inclusions were quantified using the macro script or Cell Counter on the FIJI software. Data are mean ± SEM of at least 2 independent biological replicates. To quantify production of infectious progeny, infected HeLa cells were osmotically lysed in ddH2O at 48 hpi. 2- to 5-fold serial dilutions of harvested bacteria were used to infect fresh HeLa monolayers. After removal of infection media, fresh media containing 1 mg/mL Heparin (Sigma) was added to cells. At 24 hpi, inclusion formation was enumerated as described above.

Quantitation of protein co-localization

Co-localization of GFP-STX7, mCherry-STX12, and endogenous SNX6 vesicles during L2 infection was quantified by fluorescence microscopy. HeLa cells co-transfected with GFP-STX7 and mCherry-STX12 were infected with indicated L2 strain, fixed, and permeabilized. Cells were incubated with anti-SNX6, anti-IncA, anti-STX12, and fluorescent secondary antibodies. Images were acquired using a 60X objective lens. A total of 10–15 fields per coverslip x 3 technical replicates were acquired. The fluorescence intensity profiles for GFP-STX7, mCherry-STX12, and endogenous SNX6 were generated using the FIJI software. The maximum fluorescent intensity (F_{max}) for SNX6 was arbitrarily set to position zero. The maximum fluorescent intensity offsets for STX7 and STX12 from SNX6 were computed and converted to microns (1 arbitrary unit = 0.09 μm) using the following equation:

$$\text{Offset Distance} = \text{I(SNX6 } F_{max} \text{ Position} - \text{STX7/12 } F_{max} \text{ Position)(0.09 } \mu\text{m)I}$$

STX7 or STX12 were considered to co-localize with SNX6 when the F_{max} offset distance was ≤0.09μm. STX7 or STX12 were score as not co-localizing with SNX6 is when the F_{max} offset distance was >0.09μm. Data are mean ± SD of 30 vesicles.

Statistical analysis: For each experiment, at least 2 or more independent biological/technical replicates were performed, and the results are plotted individually or combined and represented as mean ± SD/SEM, as described in the figure legends. All statistical analyses were performed using GraphPad Prism 9.0. Assays were analyzed using a one-way ANOVA with a two-tailed Welch's t test or unpaired Student t-test.

Supplementary Material

Refer to Web version on PubMed Central for supplementary material.

ACKNOWLEDGMENTS

We thank Drs. Ted Hackstadt, Dan Rockey, Isabelle Derré, Sourav Bandyopadhyay, and Kenneth Fields for reagents. This work was supported by grants from the NIH (NIAID RO1AI1163526, RO1AI122747, and R56AI152526 to J.N.E. and NIAID F32AI133902 to K.P.).

REFERENCES

1. Hocking JS, Geisler WM, and Kong FYS (2023). Update on the Epidemiology, Screening, and Management of Chlamydia trachomatis Infection. Infect. Dis. Clin. North Am 37, 267–288. 10.1016/j.idc.2023.02.007. [PubMed: 37005162]

2. Elwell C, Mirrashidi K, and Engel J (2016). Chlamydia cell biology and pathogenesis. Nat. Rev. Microbiol 14, 385–400. 10.1038/nrmicro.2016.30. [PubMed: 27108705]

3. Rockey DD, Scidmore MA, Bannantine JP, and Brown WJ (2002). Proteins in the chlamydial inclusion membrane. Microbes Infect. 4, 333–340. [PubMed: 11909744]

4. Mirrashidi KM, Elwell CA, Verschueren E, Johnson JR, Frando A, Von Dollen J, Rosenberg O, Gulbahce N, Jang G, Johnson T, et al. (2015). Global Mapping of the Inc-Human Interactome Reveals that Retromer Restricts Chlamydia Infection. Cell Host Microbe 18, 109–121. 10.1016/j.chom.2015.06.004. [PubMed: 26118995]

5. Simonetti B, Paul B, Chaudhari K, Weeratunga S, Steinberg F, Gorla M, Heesom KJ, Bashaw GJ, Collins BM, and Cullen PJ (2019). Molecular identification of a BAR domain-containing coat complex for endosomal recycling of transmembrane proteins. Nat. Cell Biol 21, 1219–1233. 10.1038/s41556-019-0393-3. [PubMed: 31576058]

6. Seaman MNJ (2021). The Retromer Complex: From Genesis to Revelations. Trends Biochem. Sci 46, 608–620. 10.1016/j.tibs.2020.12.009. [PubMed: 33526371]

7. Elwell CA, Czudnochowski N, von Dollen J, Johnson JR, Nakagawa R, Mirrashidi K, Krogan NJ, Engel JN, and Rosenberg OS (2017). Chlamydia interfere with an interaction between the mannose-6-phosphate receptor and sorting nexins to counteract host restriction. Elife 6, e22709. 10.7554/eLife.22709.

8. Yong X, Zhao L, Deng W, Sun H, Zhou X, Mao L, Hu W, Shen X, Sun Q, Billadeau DD, et al. (2020). Mechanism of cargo recognition by retromer-linked SNX-BAR proteins. PLoS Biol. 18, e3000631. 10.1371/journal.pbio.3000631.

9. Paul B, Kim HS, Kerr MC, Huston WM, Teasdale RD, and Collins BM (2017). Structural basis for the hijacking of endosomal sorting nexin proteins by Chlamydia trachomatis. Elife 6, e22311. 10.7554/eLife.22311.

10. Sun Q, Yong X, Sun X, Yang F, Dai Z, Gong Y, Zhou L, Zhang X, Niu D, Dai L, et al. (2017). Structural and functional insights into sorting nexin 5/6 interaction with bacterial effector IncE. Signal Transduct. Target. Ther 2, 17030. [PubMed: 29263922]

11. Aeberhard L, Banhart S, Fischer M, Jehmlich N, Rose L, Koch S, Laue M, Renard BY, Schmidt F, and Heuer D (2015). The Proteome of the Isolated Chlamydia trachomatis Containing Vacuole Reveals a Complex Trafficking Platform Enriched for Retromer Components. PLoS Pathog. 11, e1004883. 10.1371/journal.ppat.1004883.

12. Collins RF, Schreiber AD, Grinstein S, and Trimble WS (2002). Syntaxins 13 and 7 function at distinct steps during phagocytosis. J. Immunol 169, 3250–3256. 10.4049/jimmunol.169.6.3250. [PubMed: 12218144]

13. West ZE, Aitcheson SM, Semmler ABT, and Murray RZ (2021). The trans-SNARE complex VAMP4/Stx6/Stx7/Vti1b is a key regulator of Golgi to late endosome MT1-MMP transport in macrophages. Traffic 22, 368–376. 10.1111/tra.12813. [PubMed: 34476885]

14. Hong W (2005). SNAREs and traffic. Biochim. Biophys. Acta 1744, 493–517. [PubMed: 16038056]

15. Bonifacino JS, and Glick BS (2004). The mechanisms of vesicle budding and fusion. Cell 116, 153–166. [PubMed: 14744428]

16. Fasshauer D, Sutton RB, Brunger AT, and Jahn R (1998). Conserved structural features of the synaptic fusion complex: SNARE proteins reclassified as Q- and R-SNAREs. Proc. Natl. Acad. Sci. USA 95, 15781–15786. 10.1073/pnas.95.26.15781. [PubMed: 9861047]

17. Sutton RB, Fasshauer D, Jahn R, and Brunger AT (1998). Crystal structure of a SNARE complex involved in synaptic exocytosis at 2.4 A resolution. Nature 395, 347–353. 10.1038/26412. [PubMed: 9759724]

18. Simonetti B, Daly JL, and Cullen PJ (2023). Out of the ESCPE room: Emerging roles of endosomal SNX-BARs in receptor transport and host-pathogen interaction. Traffic 24, 234–250. 10.1111/tra.12885. [PubMed: 37089068]

19. van Ooij C, Homola E, Kincaid E, and Engel J (1998). Fusion of vacuoles containing *Chlamydia trachomatis* is inhibited at low temperature and requires bacterial protein synthesis. Infect. Immun 66, 5364–5371. [PubMed: 9784545]

20. Barnes RC, Suchland RJ, Wang S-P, Kuo C-C, and Stamm WE (1985). Detection of Multiple Serovars of Chlamydia trachomatis in Genital Infections. J. Infect. Dis 152, 985–989. 10.1093/infdis/152.5.985. [PubMed: 3840190]
21. Geisler WM, Suchland RJ, Rockey DD, and Stamm WE (2001). Epidemiology and clinical manifestations of unique Chlamydia trachomatis isolates that occupy nonfusogenic inclusions. J. Infect. Dis 184, 879–884. [PubMed: 11528595]
22. Suchland RJ, Rockey DD, Bannantine JP, and Stamm WE (2000). Isolates of Chlamydia trachomatis that occupy nonfusogenic inclusions lack IncA, a protein localized to the inclusion membrane. Infect. Immun 68, 360–367. [PubMed: 10603409]
23. Suchland RJ, Jeffrey BM, Xia M, Bhatia A, Chu HG, Rockey DD, and Stamm WE (2008). Identification of concomitant infection with Chlamydia trachomatis IncA-negative mutant and wild-type strains by genomic, transcriptional, and biological characterizations. Infect. Immun 76, 5438–5446. 10.1128/IAI.00984-08. [PubMed: 18852248]
24. Johnson CM, and Fisher DJ (2013). Site-specific, insertional inactivation of incA in Chlamydia trachomatis using a group II intron. PLoS One 8, e83989. 10.1371/journal.pone.0083989. [PubMed: 24391860]
25. Weber MM, Noriea NF, Bauler LD, Lam JL, Sager J, Wesolowski J, Paumet F, and Hackstadt T (2016). A Functional Core of IncA Is Required for Chlamydia trachomatis Inclusion Fusion. J. Bacteriol 198, 1347–1355. 10.1128/JB.00933-15. [PubMed: 26883826]
26. Klumperman J, and Raposo G (2014). The complex ultrastructure of the endolysosomal system. Cold Spring Harb. Perspect. Biol 6, a016857. 10.1101/cshperspect.a016857.
27. Mullock BM, Smith CW, Ihrke G, Bright NA, Lindsay M, Parkinson EJ, Brooks DA, Parton RG, James DE, Luzio JP, and Piper RC (2000). Syntaxin 7 is localized to late endosome compartments, associates with Vamp 8, and Is required for late endosome-lysosome fusion. Mol. Biol. Cell 11, 3137–3153. 10.1091/mbc.11.9.3137. [PubMed: 10982406]
28. Tang BL, Tan AE, Lim LK, Lee SS, Low DY, and Hong W. (1998). Syntaxin 12, a member of the syntaxin family localized to the endosome. J. Biol. Chem 273, 6944–6950. [PubMed: 9507000]
29. Dingjan I, Linders PTA, Verboogen DRJ, Revelo NH, Ter Beest M, and van den Bogaart G. (2018). Endosomal and Phagosomal SNAREs. Physiol. Rev 98, 1465–1492. 10.1152/physrev.00037.2017. [PubMed: 29790818]
30. Prekeris R, Klumperman J, Chen YA, and Scheller RH (1998). Syntaxin 13 mediates cycling of plasma membrane proteins via tubulovesicular recycling endosomes. J. Cell Biol 143, 957–971. 10.1083/jcb.143.4.957. [PubMed: 9817754]
31. Pryor PR, Mullock BM, Bright NA, Lindsay MR, Gray SR, Richardson SCW, Stewart A, James DE, Piper RC, and Luzio JP (2004). Combinatorial SNARE complexes with VAMP7 or VAMP8 define different late endocytic fusion events. EMBO Rep. 5, 590–595. 10.1038/sj.embor.7400150. [PubMed: 15133481]
32. Parveen S, Khamari A, Raju J, Coppolino MG, and Datta S. (2022). Syntaxin 7 contributes to breast cancer cell invasion by promoting invadopodia formation. J. Cell Sci 135, jcs259576. 10.1242/jcs.259576.
33. Ganley IG, Espinosa E, and Pfeffer SR (2008). A syntaxin 10-SNARE complex distinguishes two distinct transport routes from endosomes to the trans-Golgi in human cells. J. Cell Biol 180, 159–172. 10.1083/jcb.200707136. [PubMed: 18195106]
34. Arighi CN, Hartnell LM, Aguilar RC, Haft CR, and Bonifacino JS (2004). Role of the mammalian retromer in sorting of the cation-independent mannose 6-phosphate receptor. J. Cell Biol 165, 123–133. 10.1083/jcb.200312055. [PubMed: 15078903]
35. Bared SM, Buechler C, Boettcher A, Dayoub R, Sigruener A, Grandl M, Rudolph C, Dada A, and Schmitz G. (2004). Association of ABCA1 with syntaxin 13 and flotillin-1 and enhanced phagocytosis in tangier cells. Mol. Biol. Cell 15, 5399–5407. 10.1091/mbc.e04-03-0182. [PubMed: 15469992]
36. Carabeo RA, Mead DJ, and Hackstadt T. (2003). Golgi-dependent transport of cholesterol to the *Chlamydial* inclusion. Proc. Natl. Acad. Sci. USA 100, 6771–6776. [PubMed: 12743366]

37. Kumar M, Michael S, Alvarado-Valverde J, Mészáros B, Sámano-Sánchez H, Zeke A, Dobson L, Lazar T, Örd M, Nagpal A, et al. (2022). The Eukaryotic Linear Motif resource: 2022 release. Nucleic Acids Res. 50, D497–D508. 10.1093/nar/gkab975. [PubMed: 34718738]
38. Tompa P, Davey NE, Gibson TJ, and Babu MM (2014). A million peptide motifs for the molecular biologist. Mol. Cell 55, 161–169. 10.1016/j.molcel.2014.05.032. [PubMed: 25038412]
39. Madhu P, Davey NE, and Ivarsson Y. (2022). How viral proteins bind short linear motifs and intrinsically disordered domains. Essays Biochem. 10.1042/EBC20220047.
40. Davey NE, Travé G, and Gibson TJ (2011). How viruses hijack cell regulation. Trends Biochem. Sci 36, 159–169. 10.1016/j.tibs.2010.10.002. [PubMed: 21146412]
41. Samano-Sanchez H, and Gibson TJ (2020). Mimicry of Short Linear Motifs by Bacterial Pathogens: A Drugging Opportunity. Trends Biochem. Sci 45, 526–544. 10.1016/j.tibs.2020.03.003. [PubMed: 32413327]
42. Katz L, and Brennwald P. (2000). Testing the 3Q:1R "rule": mutational analysis of the ionic "zero" layer in the yeast exocytic SNARE complex reveals no requirement for arginine. Mol. Biol. Cell 11, 3849–3858. 10.1091/mbc.11.11.3849. [PubMed: 11071911]
43. Sherry J, Dolat L, Mcmahon E, Swaney DL, Bastidas RJ, Johnson JR, Valdivia RH, Krogan NJ, Elwell CA, and Engel JN (2022). Chlamydia trachomatis effector Dre1 interacts with dynactin to reposition host organelles during infection. Bioxriv. 10.1101/2022.04.15.488217.
44. Murray R, Flora E, Bayne C, and Derré I. (2017). IncV, a FFAT motif-containing Chlamydia protein, tethers the endoplasmic reticulum to the pathogen-containing vacuole. Proc. Natl. Acad. Sci. USA 114, 12039–12044. 10.1073/pnas.1709060114. [PubMed: 29078338]
45. Lutter EI, Martens C, and Hackstadt T. (2012). Evolution and Conservation of Predicted Inclusion Membrane Proteins in Chlamydiae. Int. J. Genom 2012, 362104. 10.1155/2012/362104.
46. Neduva V, and Russell RB (2005). Linear motifs: evolutionary interaction switches. FEBS Lett. 579, 3342–3345. 10.1016/j.febslet.2005.04.005. [PubMed: 15943979]
47. Davey NE, Cyert MS, and Moses AM (2015). Short linear motifs - ex nihilo evolution of protein regulation. Cell Commun. Signal 13, 43. 10.1186/s12964-015-0120-z. [PubMed: 26589632]
48. Bannantine JP, Stamm WE, Suchland RJ, and Rockey DD (1998). Chlamydia trachomatis IncA is localized to the inclusion membrane and is recognized by antisera from infected humans and primates. Infect. Immun 66, 6017–6021. [PubMed: 9826388]
49. Scidmore-Carlson MA, Shaw EI, Dooley CA, Fischer ER, and Hackstadt T. (1999). Identification and characterization of a Chlamydia trachomatis early operon encoding four novel inclusion membrane proteins. Mol. Microbiol 33, 753–765. 10.1046/j.1365-2958.1999.01523.x. [PubMed: 10447885]
50. Davis ZH, Verschueren E, Jang GM, Kleffman K, Johnson JR, Park J, Von Dollen J, Maher MC, Johnson T, Newton W, et al. (2015). Global Mapping of Herpesvirus-Host Protein Complexes Reveals a Transcription Strategy for Late Genes. Mol. Cell 57, 349–360. 10.1016/j.molcel.2014.11.026. [PubMed: 25544563]
51. Nunes A, Gomes JP, Mead S, Florindo C, Correia H, Borrego MJ, and Dean D. (2007). Comparative expression profiling of the Chlamydia trachomatis pmp gene family for clinical and reference strains. PLoS One 2, e878. 10.1371/journal.pone.0000878. [PubMed: 17849007]
52. Agaisse H, and Derré I. (2013). A C. trachomatis cloning vector and the generation of C. trachomatis strains expressing fluorescent proteins under the control of a C. trachomatis promoter. PLoS One 8, e57090. 10.1371/journal.pone.0057090. [PubMed: 23441233]
53. Keb G, Hayman R, and Fields KA (2018). Floxed-Cassette Allelic Exchange Mutagenesis Enables Markerless Gene Deletion in Chlamydia trachomatis and Can Reverse Cassette-Induced Polar Effects. J. Bacteriol 200, e00479–18. 10.1128/JB.00479-18.
54. Jager S, Cimermancic P, Gulbahce N, Johnson JR, McGovern KE, Clarke SC, Shales M, Mercenne G, Pache L, Li K, et al. (2011). Global landscape of HIV-human protein complexes. Nature 481, 365–370. 10.1038/nature10719. [PubMed: 22190034]
55. Yang X, Boehm JS, Yang X, Salehi-Ashtiani K, Hao T, Shen Y, Lubonja R, Thomas SR, Alkan O, Bhimdi T, et al. (2011). A public genome-scale lentiviral expression library of human ORFs. Nat. Methods 8, 659–661. 10.1038/nmeth.1638. [PubMed: 21706014]

56. Schindelin J, Arganda-Carreras I, Frise E, Kaynig V, Longair M, Pietzsch T, Preibisch S, Rueden C, Saalfeld S, Schmid B, et al. (2012). Fiji: an open-source platform for biological-image analysis. Nat. Methods 9, 676–682. 10.1038/nmeth.2019. [PubMed: 22743772]

57. Elwell CA, Jiang S, Kim JH, Lee A, Wittmann T, Hanada K, Melancon P, and Engel JN (2011). Chlamydia trachomatis Co-opts GBF1 and CERT to Acquire Host Sphingomyelin for Distinct Roles during Intracellular Development. PLoS Pathog. 7, e1002198. 10.1371/journal.ppat.1002198.

58. Wang Y, Kahane S, Cutcliffe LT, Skilton RJ, Lambden PR, and Clarke IN (2011). Development of a transformation system for Chlamydia trachomatis: restoration of glycogen biosynthesis by acquisition of a plasmid shuttle vector. PLoS Pathog. 7, e1002258. 10.1371/journal.ppat.1002258.

59. Tusnady GE, and Simon I. (1998). Principles governing amino acid composition of integral membrane proteins: application to topology prediction. J. Mol. Biol 283, 489–506. 10.1006/jmbi.1998.2107. [PubMed: 9769220]

60. Hofmann K, and Stoffel W. (1993). TMbase-a database of membrane spanning proteins segments. Biol. Chem. Hoppe Seyler 347, 166.

61. Hirokawa T, Boon-Chieng S, and Mitaku S. (1998). SOSUI: classification and secondary structure prediction system for membrane proteins. Bioinformatics 14, 378–379. 10.1093/bioinformatics/14.4.378. [PubMed: 9632836]

62. Madeira F, Pearce M, Tivey ARN, Basutkar P, Lee J, Edbali O, Madhusoodanan N, Kolesnikov A, and Lopez R. (2022). Search and sequence analysis tools services from EMBL-EBI in 2022. Nucleic Acids Res. 50, W276–W279. 10.1093/nar/gkac240. [PubMed: 35412617]

Highlights

- *Chlamydia* IncE encodes two SLiMs required for intracellular growth
- SLiM1 mimics an R-SNARE to bind STX7/STX12; SLiM2 mimics a SNX cargo motif to bind SNX5/SNX6
- The SLiMs enable IncE to simultaneously bind STX7/STX12- and SNX5/SNX6-associated vesicles
- STX7 and STX12 serve distinct roles in the *C. trachomatis* intracellular life cycle

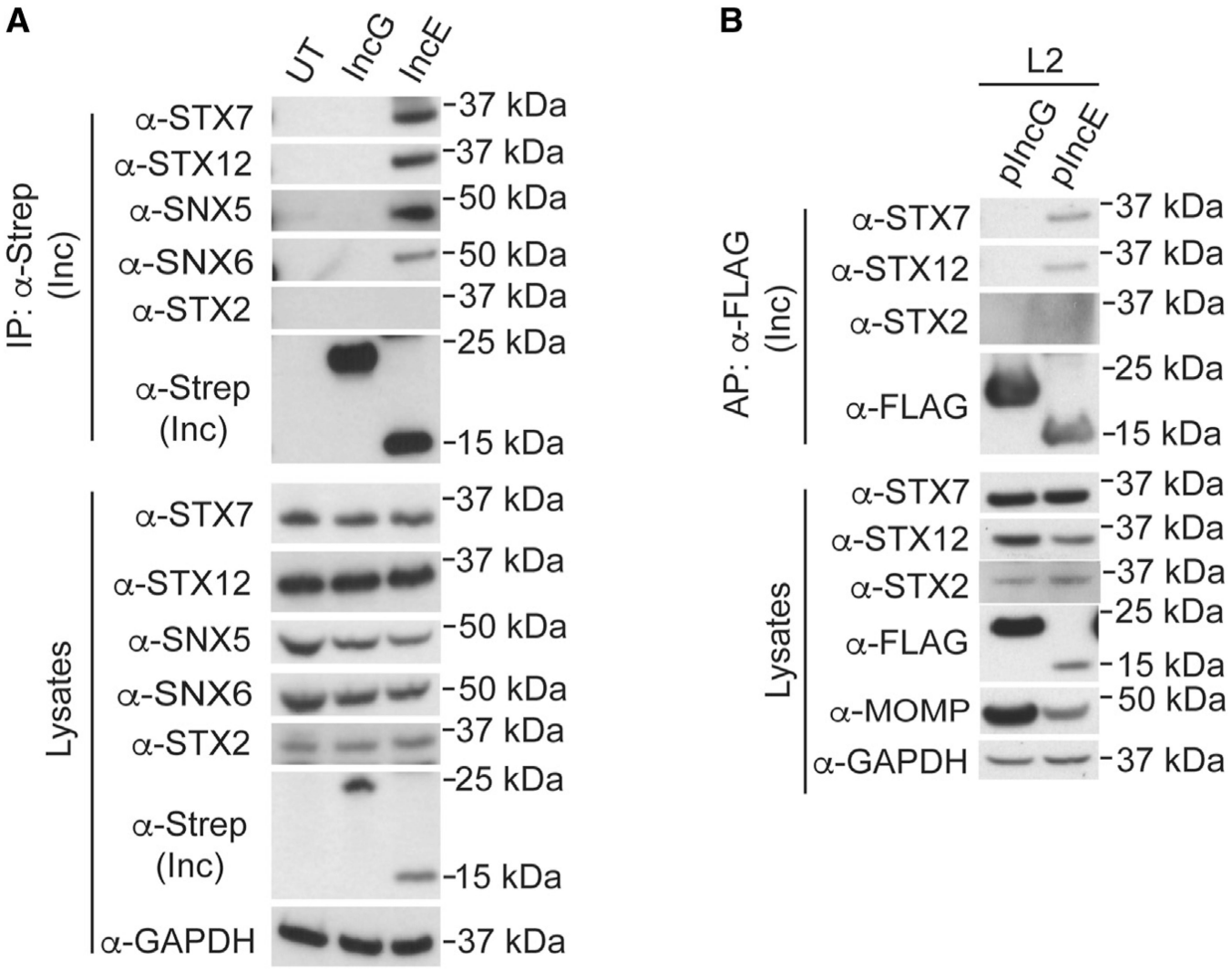

Figure 1. IncE binds specifically to STX7 and STX12

Co-APs of lysates from (A) HEK293T cells transfected with $IncG_{Strep}$ or $IncE_{Strep}$ or (B) HeLa cells infected with L2+pIncG$_{FLAG}$ or L2+pIncE$_{FLAG}$ in the presence of inducer. The unrelated STX2 serves as a control for binding specificity. GAPDH serves as a loading control. MOMP, a *Ct* protein, serves as an indicator of the efficiency of infection.

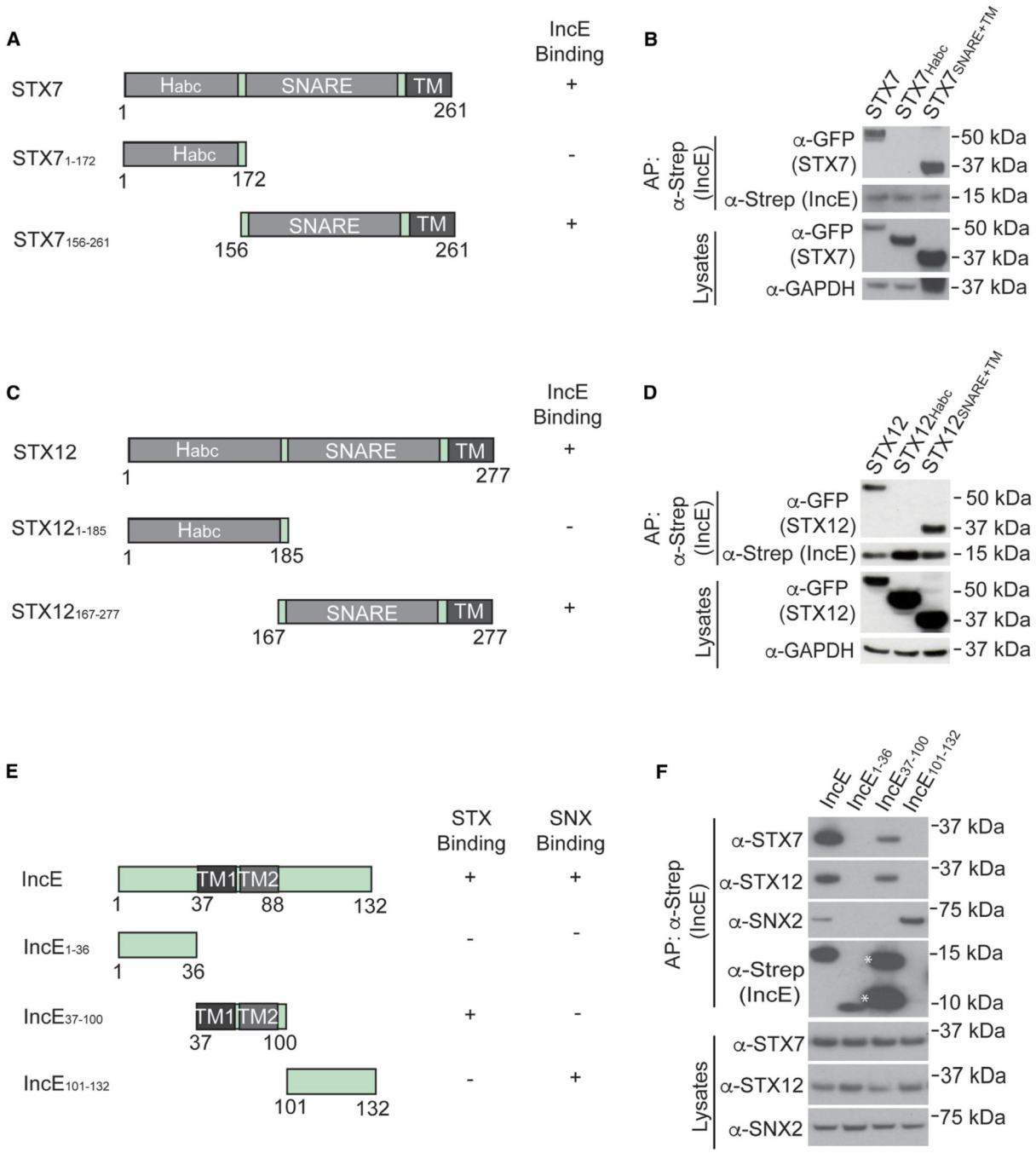

Figure 2. Defining the binding interface of STX7, STX12, and IncE

(A, C, and E) Schematic of (A) STX7, (C) STX12, and (E) IncE constructs. H_{abc}, regulatory domain; TM, transmembrane.

(B and D) Co-AP of transfected $IncE_{Strep}$ with transfected (B) GFP-STX7 or (D) GFP-STX12 deletion constructs. GAPDH serves as a loading control.

(F) Co-AP of transfected $IncE_{Strep}$ constructs with endogenous STX7, STX12, or SNX2. IncE monomers and dimers are indicated by an asterisk. SNX2 serves as a loading control

as well as a positive control for the ESCPE-1 complex (composed of SNX1/2/5/6).[18] Data shown are representative of immunoblots from two biological replicates.

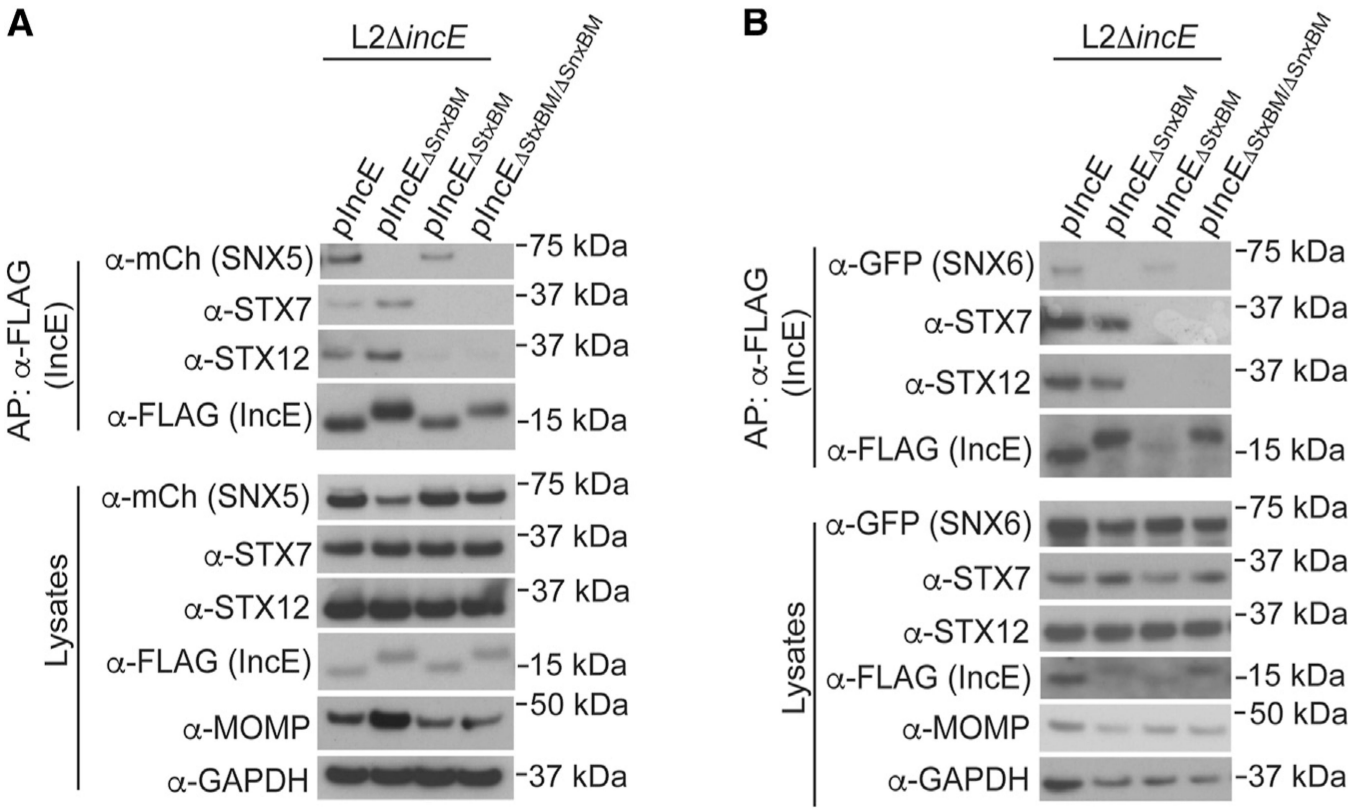

Figure 3. The IncE StxBM and SnxBM are non-overlapping

(A and B) Co-APs of lysates from HeLa cells infected with L2*ΔincE* expressing the indicated IncE constructs with (A) mCherry-SNX5, STX7, and STX12 or (B) GFP-SNX6, STX7, and STX12. Data shown are representative of immunoblots from three biological replicates. GAPDH serves as a loading control. MOMP serves as an indicator of the efficiency of infection.

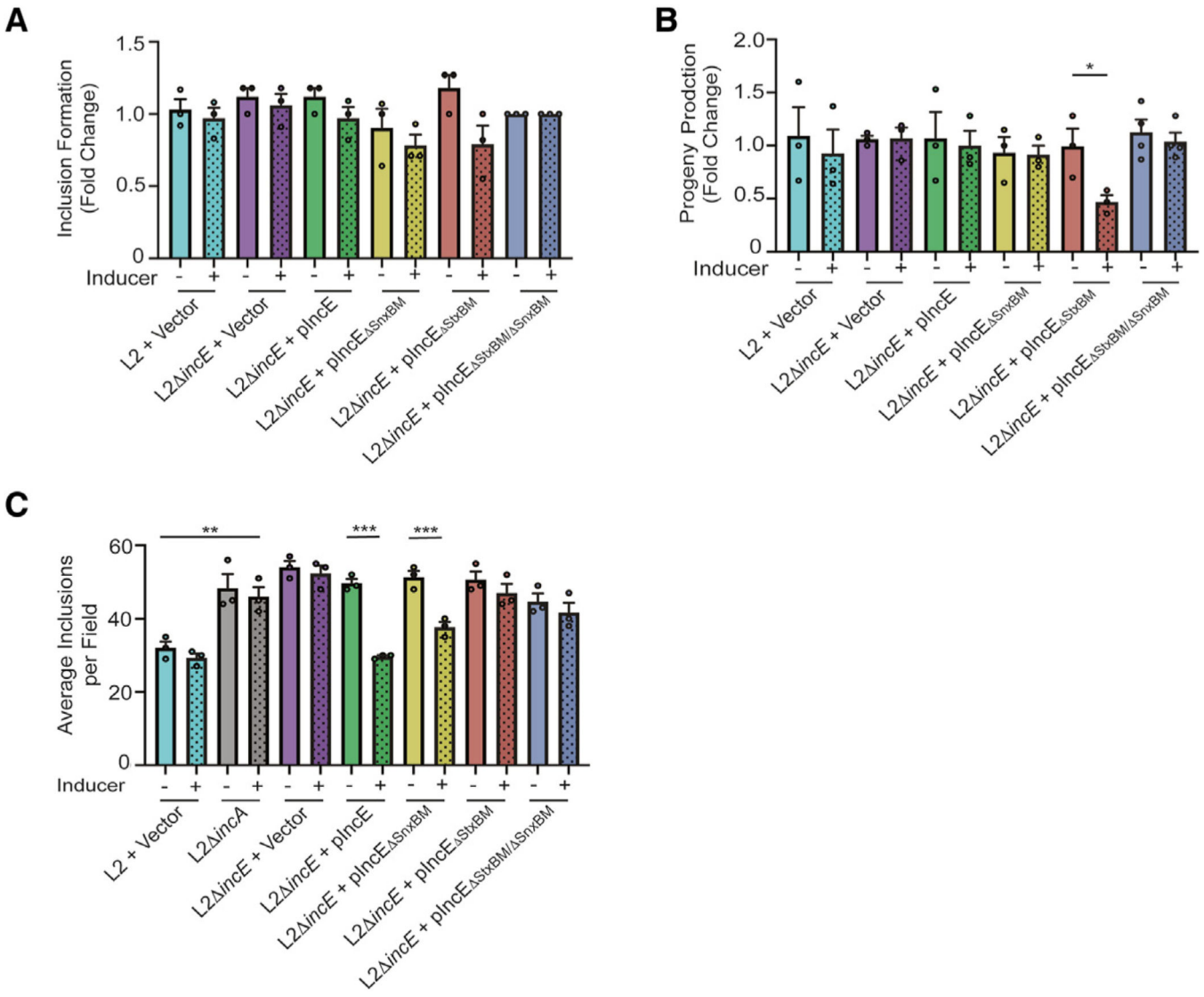

Figure 4. IncE StxBM is required for late steps of infection

(A and B) Intra-strain comparisons of (A) inclusion formation at 24 hpi and (B) progeny production at 48 hpi. Infections were performed at a low MOI (MOI = 1) and compared to the indicated strain without an inducer.

(C) Inter- and intra-strain quantification of inclusion fusion at 24 hpi. Infections were performed at a high MOI (MOI = 5). Data shown are averages ± SEM for at least three biological replicates (indicated with circle), with at least 99 fields counted for each replicate. $*p < 0.05$, $**p < 0.02$, and $***p < 0.0005$; Welch's ANOVA.

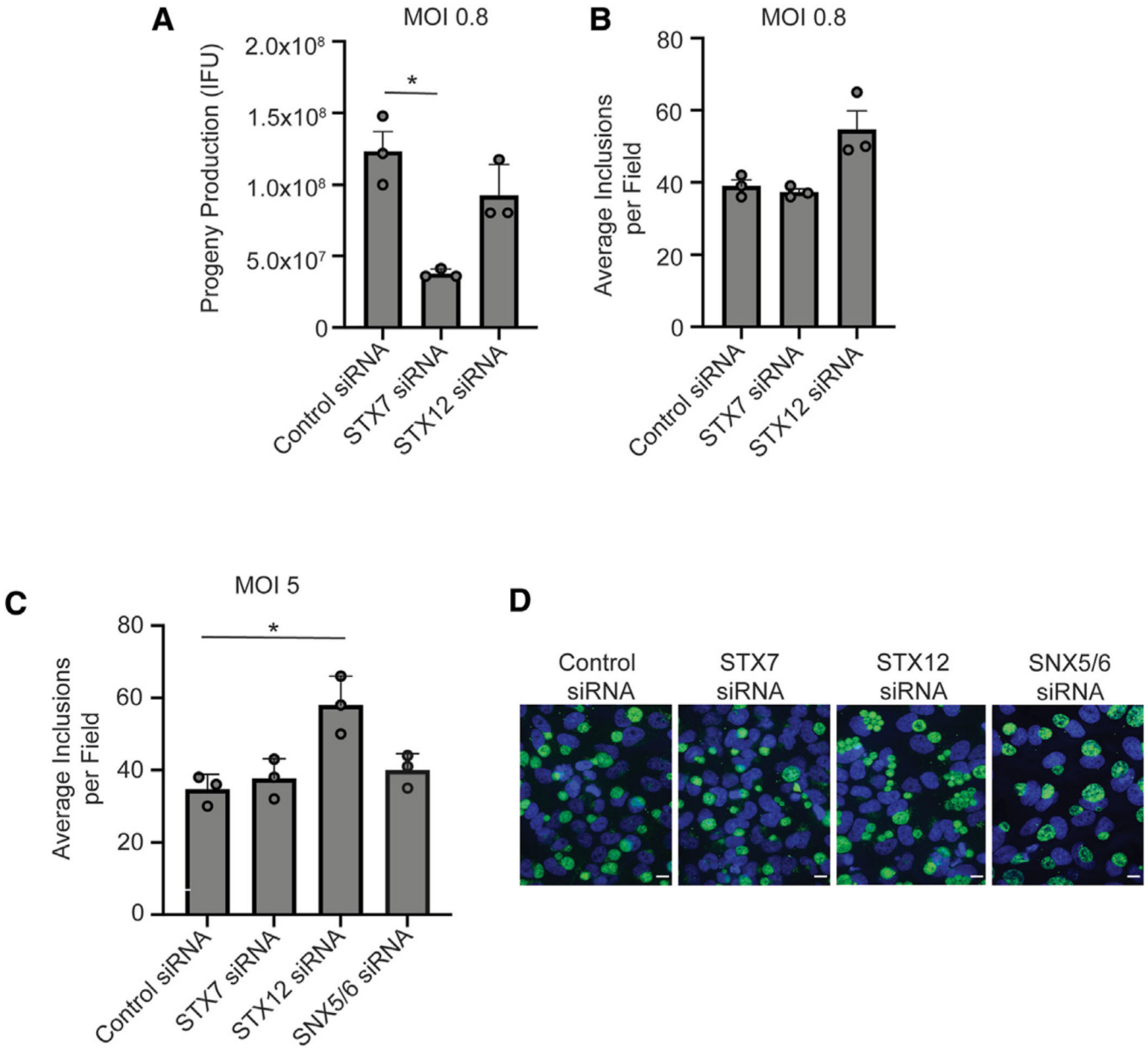

Figure 5. STX7 and STX12 serve distinct functions during infection

Control small interfering RNA (siRNA)-, STX7 siRNA-, or STX12 siRNA-depleted cells infected at a low MOI (~0.8, A and B) or high MOI (~5, C and D) for 24 h. Quantification of (A) progeny production and (B and C) average inclusions per field. (A and B) Shown is the average ± SEM for three technical replicates with a total of 33 fields. (C) Data shown are averages ± SEM for three biological replicates, with a total of 99 fields counted. The decreased inclusion fusion in the STX12 siRNA-treated cells is reflected by an increase in the average number of inclusions per field. (D) Representative single-slice confocal immunofluorescence images (scale bar: 10 μm). Multiple smaller unfused inclusions are present in the STX12 siRNA-treated sample. *$p < 0.05$ and **$p < 0.005$; Welch's ANOVA.

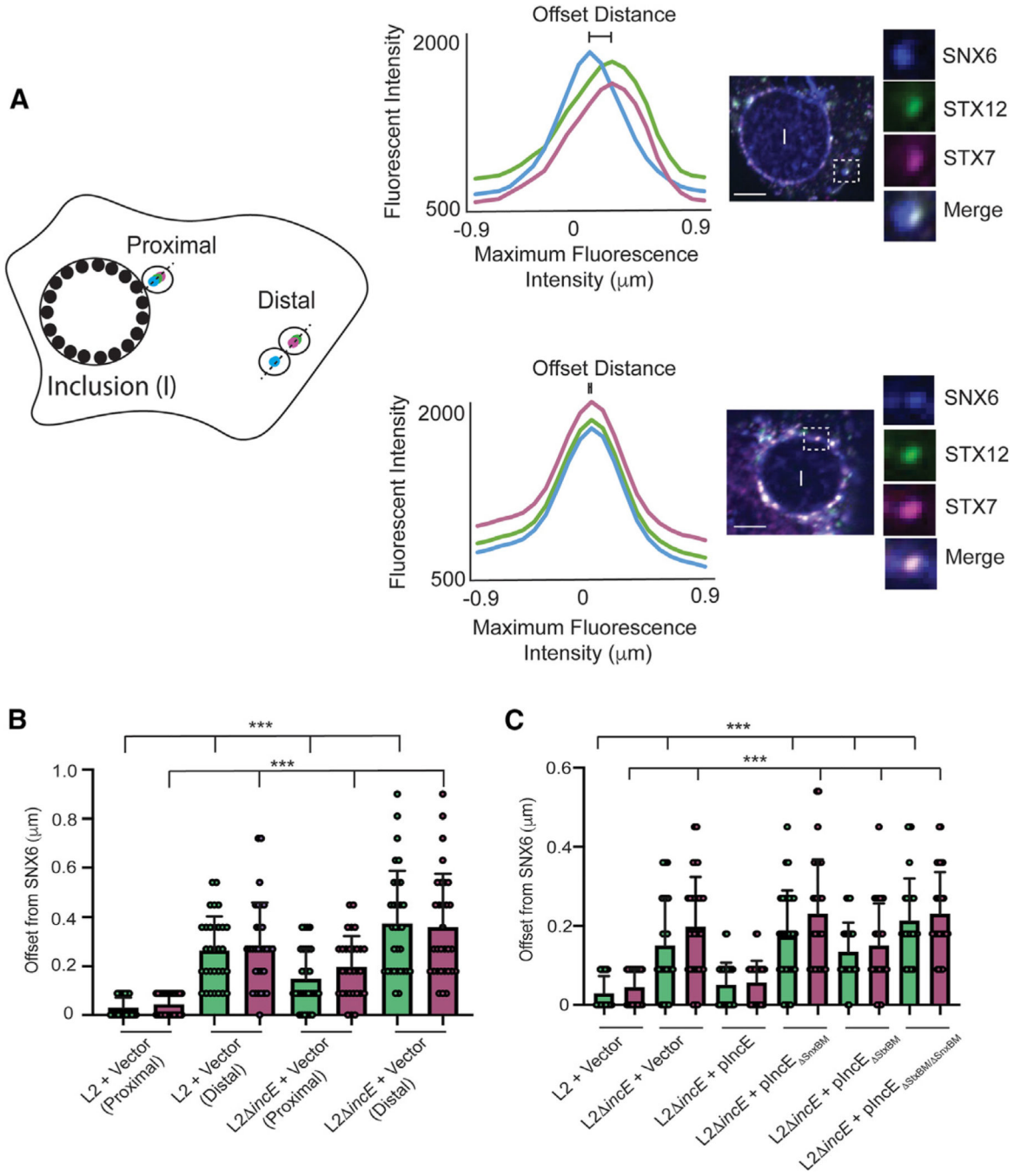

Figure 6. IncE is required to tether distinct vesicle classes together at the inclusion

(A) Schematic and representative single-slice confocal immunofluorescence images depicting quantitation of STX7/STX12/SNX6 overlap in vesicles (insets) proximal and distal to inclusion. Fluorescence profiles on vesicles proximal (≤ 1 μm) and distal (>5 μm) to the inclusion were plotted for transfected GFP-STX7 (green), transfected mCh-STX12 (magenta), and endogenous SNX6 (blue). The maximum fluorescent intensity offsets of GFP-STX7 and mCh-STX12 from SNX6 were computed. Scale bar: 5 μm.

(B and C) Quantification of STX7/SNX6 (green) and STX12/SNX6 (magenta) offset in (B) vesicles proximal or distal to inclusion in cells infected for 24 h with L2+vector or L2Δ*incE*+vector or (C) vesicles proximal to the inclusion in cells infected for 24 h with L2+vector, L2Δ*incE*+vector, or the indicated L2Δ*incE*+pIncE variants. All experiments were performed in the presence of an inducer. Shown are individual data points as well as the average ± SD for 30 vesicles for each infection condition. ***$p < 0.0005$; Welch's ANOVA.

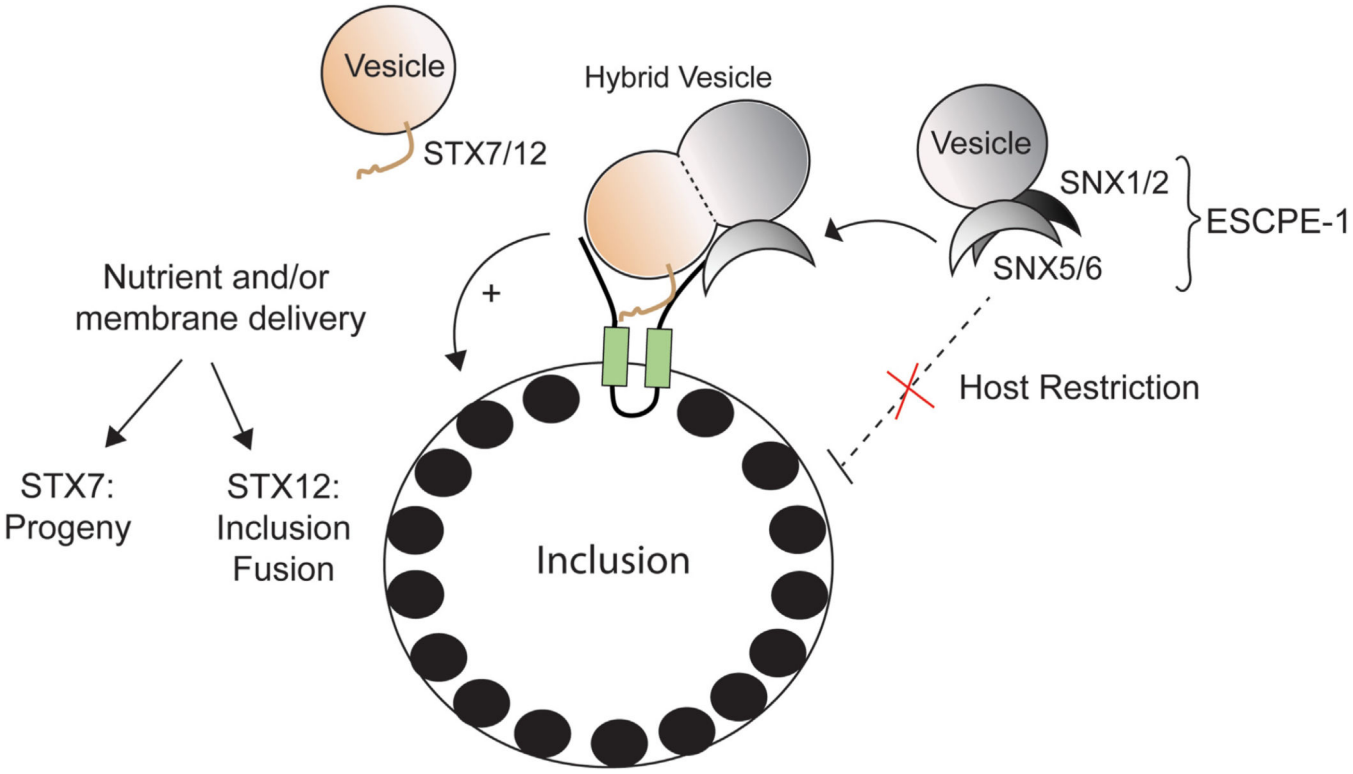

Figure 7. Model of IncE:STX7/STX12 and IncE:SNX5/SNX6 interactions

IncE encodes two SLiMs, the StxBM and SnxBM, which bind to STX7/12 and SNX5/6, respectively. The binding of the IncE SnxBM to the SNX5/6 cargo binding domain reroutes $SNX6^{+}$, and presumably $SNX5^{+}$ (gray half-moon), vesicles to the inclusion. By binding to SNX5/6, IncE displaces SNX5/6 cargo proteins and disrupts ESCPE-1-mediated restriction of *Ct* intracellular development. IncE StxBM binding to STX7 (tan squiggle line) and STX12 (tan squiggle line) reroutes STX7- and STX12-containing vesicles to the inclusion. At or near the inclusion, the STX7/12- and SNX5/6-containing vesicles are brought in close apposition in an IncE-dependent manner and may fuse with each other and/or with the inclusion membrane. STX7 contributes to the production of infectious progeny, while STX12 functions to promote efficient inclusion fusion.

KEY RESOURCES TABLE

REAGENT or RESOURCE	SOURCE	IDENTIFIER
Antibodies		
Mouse anti-STX7	Santa Cruz Biotechnology Inc	sc-514157
Rabbit anti-STX12	Atlas Antibodies	HPA055300; RRID:AB_2682778
Rabbit anti-STX2	Abcam	AB12369–1001; RRID:AB_299052
Rabbit anti-SNX5	Proteintech	17918–1-AP; RRID:AB-2192708
Mouse anti-SNX6	Santa Cruz Biotechnology Inc	sc-365965; RRID:AB_10842310
Goat anti-SNX6	Santa Cruz Biotechnology Inc	sc-8679; RRID:AB_2192723
Mouse anti-FLAG	Sigma	F3165; RRID:AB_259529
Rabbit anti-FLAG	Sigma	F7425; RRID:AB_439687
Mouse anti-GAPDH	Millipore	MAB374; RRID:AB_2107445
Goat anti-MOMP L2	Fitzgerald	20C-CR2104GP; RRID:AB_1283809
Rabbit anti-Strep TagII HRP	Millipore	71591–3; RRID:AB_10806716
Mouse anti-GFP	Roche	11814460001; RRID:AB_390913
Rabbit anti-RFP	Rockland	600–401-379-RTU; RRID:AB_2209751
Mouse anti-IncA	Rockey Group; Bannantine et al.[48]	https://doi.org/10.1128/2Fiai.66.12.6017-6021.1998
Rabbit anti-IncG	Hackstadt Group; Scidmore-Carlson et al.[49]	https://doi.org/10.1046/j.1365-2958.1999.01523.x
Rabbit anti-IncE	Hackstadt Group; Scidmore-Carlson et al.[49]	https://doi.org/10.1046/j.1365-2958.1999.01523.x
Rabbit anti-IncE	Genscript	This Paper
Mouse anti-HSP60	Santa Cruz Biotechnology Inc	sc-57840; RRID:AB_783868
Mouse anti-FLAG magnetic beads	Sigma	M8823; RRID:AB_2637089
Donkey anti-goat Alexa Fluor 647	Life Technologies	A21447; RRID:AB_253586
Donkey anti-mouse Alexa Fluor 647	Life Technologies	A31571; RRID:AB_162542
Donkey anti-mouse Alexa Fluor 568	Life Technologies	A10037; RRID:AB_111808
Donkey anti-rabbit Alexa Fluor 568	Life Technologies	A10042; RRID:AB_253401
Donkey anti-goat Alexa Fluor 488	Life Technologies	A11055; RRID:AB_253410
Donkey anti-rabbit Alexa Fluor 488	Life Technologies	A21206; RRID:AB_253579
Donkey anti-mouse Alexa Fluor 405	Life Technologies	A31556; RRID:AB_221605
Bacterial and virus strains		

REAGENT or RESOURCE	SOURCE	IDENTIFIER
Stellar *E. coli*	Takara Bio	636763
10-beta *E. coli*	New England Biolab	C3020K
dam-/dcm- *E. coli*	New Engalnd Biolab	C2925H
Chemicals, peptides, and recombinant proteins		
Heparin sodium salt	Sigma	H3393
D-desthiobiotin	IBA	2–1000-002
Strep-Tactin Sepharose beads	IBA	2–1201-010
Continuum Transfection Reagent	GeminiBio	400–700
Anhydrous tetracycline	Takara Biotech	631310
3X FLAG peptide	Sigma	F4799
Protein G Agarose beads	Pierce	20398
DharmaFECT 1 Transfection Reagent	Dharmacon	T-2001–01
Effectene	Qiagen	301425
VECTASHIELD Antifade Mounting Medium with DAPI	Vector Laboratories	H-1200–10
VECTASHIELD Antifade Mounting Medium	Vector Laboratories	H-1000–10
VECTASHIELD HardSet Antifade Mounting Medium with DAPI	Vector Laboratories	H-1500–10
Ampicillin	Sigma	A9518
Cycloheximide	Sigma	239765
Spectinomycin	Sigma	S4014
Sbf1-HF	New England Biolabs	R3642S
EagI-HF	New England Biolabs	R3505S
EcoR1-HF	New England Biolabs	R3101S
Not-HF	New England Biolabs	R3189S
HindIII-HF	New England Biolabs	R3142S
KpnI-HF	New England Biolabs	R3104S
SalI-HF	New England Biolabs	R3138S
T4 DNA Ligase	New England Biolabs	M0202S
Igepal CA-630	Sigma	I8896
Critical commercial assays		

REAGENT or RESOURCE	SOURCE	IDENTIFIER
NEBBuilder HiFi DNA Assembly Master Mix	New England Biolabs	E2621S
InFusion	Takara Biotech	638910
TargeTron	Sigma	TA0100
Lookout Mycoplasma PCR Detection Kit	Sigma	MP0035–1KT
Experimental models: cell lines		
HEK293T	Krogan Group; Davis et al.[50]	https://doi.org/10.1016/j.molcel.2014.11.026
HeLa	ATCC	CCL-2; RRID:CVCL_0030
Vero	ATCC	CCL-81; RRID:CVCL_0059
Experimental models: organisms/strains		
Chlamydia trachomatis 434/Bu (L2)	Dean Group; Nunes et al.[51]	https://doi.org/10.1371/journal.pone.0000878
L2+Vector	This Study	N/A
L2pIncE	This Study	N/A
L2pIncG	Derré Group; Agaisse and Derré[52]	https://doi.org/10.1371/journal.pone.0057090
L2Δ*incE*+Vector	This Study	N/A
L2Δ*incE*+pIncE	This Study	N/A
L2Δ*incE*+pIncE$_{\Delta StxBM}$	This Study	N/A
L2Δ*incE*+pIncE$_{\Delta SnxBM}$	This Study	N/A
L2Δ*incE*+pIncE$_{\Delta SnxBM/\Delta StxBM}$	This Study	N/A
L2Δ*incA*	Fisher Group; Johnson and Fisher[24]	https://doi.org/10.1371/journal.pone.0083989
Oligonucleotides		
IncE Forward (CAGTGTGGTGGAATTCATGGAATGCGTTAAACAGTTATGTAGAAACC)	This Study	N/A
IncE Reverse (CTCCCTCGAGCGGCCGCCCTTGAGTTACTAAAATCACTTGGTCTGCGC)	This Study	N/A
IncE 2 Forward (GTGAACGGCCGATGGAATGCGTTAAACAG)	This Study	N/A
IncE 2 Reverse (CCATCCCTGCAGGTTGAGTTACTAAAATCAC)	This Study	N/A
IncE$_{37–100}$ Forward (CAGTGTGGTGGAATTCATGGCAGCATGCTGTTTAGGAGTTGTTTG)	This Study	N/A
IncE$_{37–100}$ Reverse (CTCCCTCGAGCGGCCGCCCAAATGGACATCCCACCAAACCATGATTC)	This Study	N/A
IncE$_{101–132}$ Forward (CAGTGTGGTGGAATTCATGAAGTTGCCATGCAAATCGAGTCCAGC)	This Study	N/A

REAGENT or RESOURCE	SOURCE	IDENTIFIER
IncE$_{1–36}$ Reverse (CTCCCTCGAGCGGCCGCCCTAGCTGAACTTTTTCTGCAGTTGTTC)	This Study	N/A
IncE$_{\Delta SnxBM}$ Forward (AATCGAGTCCAGCTAATGAACCTGCTAATCAAGACTTTAAAGGTAAAAATGGAAGCGCAG)	This Study	N/A
IncE$_{\Delta SnxBM}$ Reverse (CTGCGCTTCCATTTTTACCTTTAAAGTCTTGATTAGCAGGTTCATTAGCTGGACTCGATT)	This Study	N/A
IncE$_{V89A/L90A/E91A}$ Forward (GTTTGCAACATCTGCTTTGGATGCTGCAGCGAATCATGGTTTGGTGGGATGTC)	This Study	N/A
IncE$_{V89A/L90A/E91A}$ Reverse (GACATCCCACCAAACCATGATTCGCTGCAGCATCCAAAGCAGATGTTGCAAAC)	This Study	N/A
IncE$_{N92A/H93A/G94A}$ Forward (AACATCTGCTTTGGATGCTGCAGCGGCTGCTGCTTTGGTGGGATGTCCATTTAAGTTG)	This Study	N/A
IncE$_{N92A/H93A/G94A}$ Reverse (CAACTTAAATGGACATCCCACCAAAGCAGCAGCCGCTGCAGCATCCAAAGCAGATGTT)	This Study	N/A
STX7 Forward (GAGCTCAAGCTTCGATGTCTTACACTCCAGGAGTTG)	This Study	N/A
STX7 Reverse (CGGTACCGTTCAGTGGTTCAATCCCCATATGAT)	This Study	N/A
STX7$_{1–172}$ Reverse (CGGTACCGTTCATTCTCTCTCATGAATAAGACGGAG)	This Study	N/A
STX7$_{156–261}$ Forward (GAGCTCAAGCTTCGATGCAGGATGAAGAAATTACAGAGGAT)	This Study	N/A
STX12 Forward (GAGCTCAAGCTTCGATGTCATACGGTCCCTTAGAC)	This Study	N/A
STX12 Reverse (CGGTACCGTTCACTTCGTTTTATAAACTAGCCA)	This Study	N/A
STX12$_{1–185}$ Reverse (CGGTACCGTTCATTCTCTTTCTTTAATAAGTTCCAAATC)	This Study	N/A
STX12$_{167–277}$ Forward (GAGCTCAAGCTTCGATGCAGGAGGATGAGGTGGC)	This Study	N/A
+3kb *incE* SalI Forward (TCCGTCACTGCAGGTACCGGGTAGGGAAAACTGAGCTTGCTAAAGCA)	This Study	N/A
+3kb *incE* SalI Reverse (AGGCATGATGATGAATGGTCGAAGAGCCTCCTAAAAACTCTTAAAACAGC)	This Study	N/A
−3kb *incE* SbfI Forward (AACTATACAAGTAAGACCTGCAGACAATGGGAGACGTGATGATACAGAG)	This Study	N/A
−3kb *incE* SbfI Reverse (TTTCTACGGGGTCTGACGCCCCTTAGCACCATGTTCTTCCCCTTGAAG)	This Study	N/A
incD Forward (ATGAGATCTGGCTAAAATCTGTCGAAGTG)	This Study	N/A
incD Reverse (TTAGCTCGCCCCTTTTTTACTCACC)	This Study	N/A
incF Forward (ATGGGAGACGTGATGATACAGAGCG)	This Study	N/A
incF Reverse (CTAGCACTTATTTGTAGAAGCGATCCATC)	This Study	N/A
incG Forward (ATGATCTGTTGTGACAAAGTCTTGTCGAG)	This Study	N/A

REAGENT or RESOURCE	SOURCE	IDENTIFIER
incG Reverse (TTAGAAGGAGCGTGATCGAGAACGG)	This Study	N/A
rpoD Forward (ATGCGCATGGATACGCTAGATAGTCAA)	This Study	N/A
rpoD Reverse (CTAATTTTTATAACTTTTAATCTTACCCGAACC)	This Study	N/A
siGENOME Human STX12 siRNA	Dharmacon	M-018246–01-0005
siGENOME Human STX7 siRNA	Dharmacon	M-019551–00-0005
siGENOME Non-Targeting siRNA Pool #2	Dharmacon	D-001206–14-05
siGENOME Human SNX5 siRNA	Dharmacon	M-012524–00-0005
siGENOME Human SNX5 siRNA	Dharmacon	M-017557–01-0005
Recombinant DNA		
pSUmc-*loxP-aadA-gfp*	Fields Group; Keb et al.[53]	https://doi.org/10.1128/jb.00590-18
pSU-CRE	Fields Group; Keb et al.[53]	https://doi.org/10.1128/jb.00590-18
p2TK2-mCherry	Derre Lab; Agaisse and Derré[52]	https://doi.org/10.1371/journal.pone.0057090
pcDNA4.0/2xStrepII	Krogan Group; Jager et al.[54]	https://doi.org/10.1038/nature10719
STX7	Bandyopadhyay Group; Yang et al.[55]	https://doi.org/10.1038/2Fnmeth.1638
STX12	Bandyopadhyay Group; Yang et al.[55]	https://doi.org/10.1038/2Fnmeth.1638
Software and algorithms		
FIJI	FIJI; Schindelin et al.[56]	https://doi.org/10.1038/nmeth.2019; RRID:SCR_00228
Prism 10	GraphPad	RRID:SCR_002798
NIS-Elements 4.10	Nikon	https://www.microscope.healthcare.nikon.com/products/confocal-microscopes/ax/software; RRID:SCR_014329
NIS-Elements Viewer	Nikon	https://www.microscope.healthcare.nikon.com/products/software/nis-elements/viewer
HMMTOP	Institute of Enzymology	http://www.enzim.hu/hmmtop/html/submit.php
TMpred	EMBnet	Open Software Discontinued
SOSUI	BINDS	https://harrier.nagahama-i-bio.ac.jp/sosui/mobile/
TMHMM	DTU Health Tech	https://services.healthtech.dtu.dk/services/TMHMM-2.0/; RRID:SCR_014935
Clustal Omega	EMBL-EBI	https://www.ebi.ac.uk/jdispatcher/msa/clustalo; RRID:SCR_001591

REAGENT or RESOURCE	SOURCE	IDENTIFIER
Other		
Eagle's Minimum Essential Medium	University of California, San Francisco Cell Culture Facility	CCFAC001
Dulbecco's Modified Eagle's Medium, High Glucose	University of California, San Francisco Cell Culture Facility	CCFAA005
Phosphate Buffer Saline	University of California, San Francisco Cell Culture Facility	CCFAL001
BenchMark Fetal Bovine Serum	GeminiBio	100–106
1M HEPES, pH 7.4	University of California, San Francisco Cell Culture Facility	CCFGL001
Dulbecco's Modified Eagle's Medium, High Glucose, without Phenol Red	University of California, San Francisco Cell Culture Facility	CCFAA006
Bovine Serum Albumin	Sigma	A2153
NP LDS Sample Buffer	Life Technologies	NP0007